universität wien

MASTERARBEIT / MASTER'S THESIS

Titel der Masterarbeit / Title of the Master's Thesis

„Seismic analysis of the southern Vienna Basin (Moosbrunn) and its structural evolution during the Miocene"

verfasst von / submitted by

Thomas Andreas Graf, BSc

angestrebter akademischer Grad / in partial fulfilment of the requirements for the degree of

Master of Science (MSc)

Wien, 2022 / Vienna 2022

Studienkennzahl lt. Studienblatt / degree programme code as it appears on the student record sheet:	UA 066 815
Studienrichtung lt. Studienblatt / degree programme as it appears on the student record sheet:	Masterstudium Erdwissenschaften
Betreut von / Supervisor:	Dr. Kurt Decker

Table of content

Table of figures

List of tables

Abstract

The Miocene Vienna Basin is located between the Eastern Alps and the Leitha Mountains. It has been studied for decades and interpreted as a large-scale pull-apart basin. The high-resolution 3D seismic reflection data (Moosbrunn, OMV) together with older 2D seismic lines were used in this study to interpret the structural setting of the southern part of the Vienna Basin and thickness changes within individual Miocene seismic packages. Based on the seismic data, four groups of faults were distinguished by their location, strike and character as well as six seismic packages were recognized leading to a better understanding of the Miocene fault activity in the basin. For example, growth strata were mapped within the Karpatian-Badenian interval (package) along with multiple faults, thus reflecting syn-sedimentary faulting. The thickness maps constructed for individual seismic packages show a change in depocenter locations through time. The main depocenters were located in the N to NE during the Kapatian, but shifted further north and south during the Pannonian, with no major fault activity in the NE. In addition, the seismic data exhibit changes in graben polarity along the main N-S trending fault zone. Further, the combination of 2D and 3D data allowed the identification of strike and dip of the Leopoldsdorf Fault, which is a major fault in the studied region. It branches off towards the north from another large-scale fault belonging to the major NE-SW trending Graben System within the Vienna Basin Transfer Fault (VBTF).

Zusammenfassung

Das Wiener Becken liegt zwischen den östlichen Alpen sowie dem Leitha Gebirge. Es wird seit Jahrzehnten erforscht und wird als großes pull-apart Becken interpretiert. Die hochauflösende 3D seismischen Reflektionsdaten (Moosbrunn, OMV) kombiniert mit den 2D seismischen Linien wurden in dieser Arbeit benutzt, um das strukturelle Gefüge des südlichen Wiener Beckens und die Wechsel der Mächtigkeiten innerhalb der verschiedenen Miozänen Einheiten besser zu interpretieren und zu verstehen. Basierend auf den seismischen Daten wurden vier Störungsgruppen aufgrund ihrer Örtlichkeit und deren Charakter, sowieso sechs seismische Pakete identifiziert. Growth Strata, gemeinsam mit mehreren Störungszonen, wurden innerhalb des Badenium identifiziert und zeigen syn-sedimentäre Störungsaktivitäten. Die Mächtigkeitskarten, die für die verschiedenen seismischen Pakete erstellt wurden, zeigen einen Wechsel der Lage der Depotcenter mit der Zeit. Das Hauptdepotcenter, welches während des

Karpatiums im N und NE lag, verschob sich während des Pannoniums weiter Richtung Norden und Süden, ohne größere Störungsaktivitäten im Nordosten. Ebenfalls zeigten die seismischen Daten einen Wechsel der Grabenpolarität entlang der N-S verlaufenden Störungszone. Weiters ermöglicht die Kombination aus 2D und 3D Daten eine Identifikation der strikes und dips der Leopoldsdorfstörung, einer der Hauptstörungen im untersuchten Gebiet. Diese zweigt Richtung Norden von einer anderen großen Störung ab, welche zu dem NE-SW verlaufenden Graben System innerhalb der Wiener Becken Transfer Störung gehört.

Chapter 1: Introduction

The Vienna Basin is located in Central Europe between the Eastern Alps, the Western Carpathians and the Pannonian Basin system (Figure 1) and represents one of the most studied pull-apart basins (e.g., Royden 1985, Wessely 1988, Decker 1996, Strauss et al. 2006). It formed along sinistral fault systems during Miocene times, reaches 200 km length and 50 km width (Figure 2a) and comprises up to 5.5 km of Miocene strata in the central part. The basin fill consists of terrestrial and shallow marine sediments of Early to Middle Miocene age (Seifert 1996, Strauss 2006) (Figure 3).

A detailed tectono-stratigraphic history with focus on Miocene sediments exists for the central part of the Vienna Basin (e.g., Wessely 1988, Weissenbäck 1996) and in a lesser extent for the southern part of the Vienna Basin (Strauss et al. 2006, Hinsch et al. 2005). This work has, therefore, focused on the lower to upper Miocene tectono-stratigraphic evolution of the southern part of the Vienna Basin. The aim of this work was to map the bigger fault systems as well as the individual sedimentary depocenters in detail and thus to improve the general understanding of Miocene syn-sedimentary fault activity by using high-resolution 3D seismic data supplemented with 2D regional seismic lines. The identification and grouping of major fault systems based on their structural trend, location and significance was another goal, which was achieved for a wider area than before due to the combination of 2D and 3D seismic data. The Leopoldsdorf Fault System is an example of such a fault zone, which was mapped on 2D lines and has been linked into the 3D seismic cube allowing for its exact location and relation to the large-scale NE-SW trending strike-slip fault zone.

The interpretation of the seismic horizons (Figure 6) resulted in a better and more detailed understanding of the individual seismic packages and their thicknesses, which has further led to the identification of individual depocenters throughout Miocene intervals (namely the Karpatian, Badenian, Sarmatian and Pannonian) in the southern Vienna Basin. The observed changes of basin polarity during different time periods and the observed thickness changes, corroborate with previously published literature and confirmed Miocene syn-sedimentary activity of the basin-bounding faults.

In Chapter 2, the regional setting and tectono-stratigraphic evolution of the Vienna Basin is briefly explained. Chapter 3 includes an overview of data used in this study and outlines the methodology. Chapter 4 presents the main results of this study,

including seismic data description and interpretation. Chapter 5 brings together various aspects discussed in earlier chapters and include main ideas about structural evolution of the southern Vienna Basin. Chapter 6 summarizes the main results and key conclusions of this study.

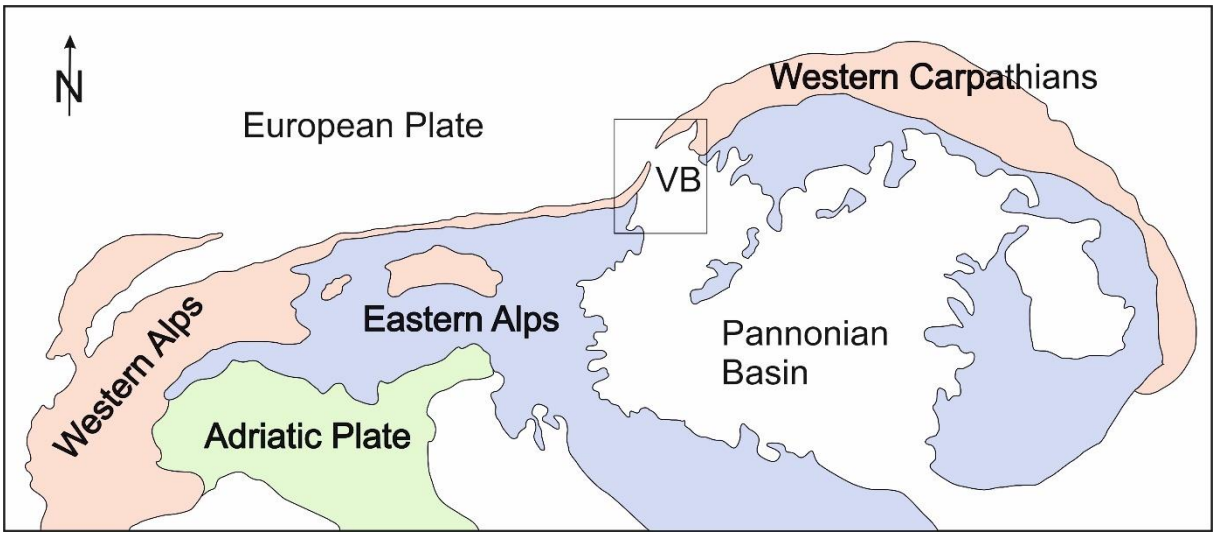

Figure 1: Tectonic sketch of the east-Alpine and west Carpathian regions showing the location of the Vienna Basin (VB) (modified from Decker & Peresson et al. 2005, Lee and Wagreich et al. 2017)

Chapter 2: Regional Setting

This chapter outlines the regional setting of the Vienna Basin and provides a general overview of the basin´s structural development during the Lower to Upper Miocene times. The Vienna Basin overlies the thin-skinned nappes of the Alpine-Carpathian thrust belt. The thrusting over the European passive margin took place during the Middle Eocene and the Early Miocene (Decker 1996). The basin has a rhombohedral shape and strikes roughly southwest-northeast, its western border is formed by the morphological eastern margin of the Northern Alps in the south and by the Waschberg Zone in the north. The eastern margin of the Vienna Basin is defined by hill ranges belonging to the Alpine-Carpathian Central Zone (Piller 1999).

The Vienna Basin is a tectonically complex basin, which has been, based on its shape and left-stepping en-echelon faults, firstly interpreted as a thin-skinned pull apart

structure (e.g., Royden 1985, Wessely et al. 1988; Figure 2). Later research showed that the basin evolution is more complex and can be divided into four main tectonic stages (e.g., Fodor 1995, Decker 1996, Peresson and Decker 1996, Decker et al. 2005, Kováč et al 2004) which are briefly summarized below. The formation and geological history of the Vienna basin includes:

1. Formation of a piggyback basin in the Lower Miocene.

2. Formation of a pull-apart basin in the Middle to Upper Miocene.

3. East-west directed compression and basin inversion in the Upper Miocene to Pliocene.

4. East-west directed extension in the Quaternary.

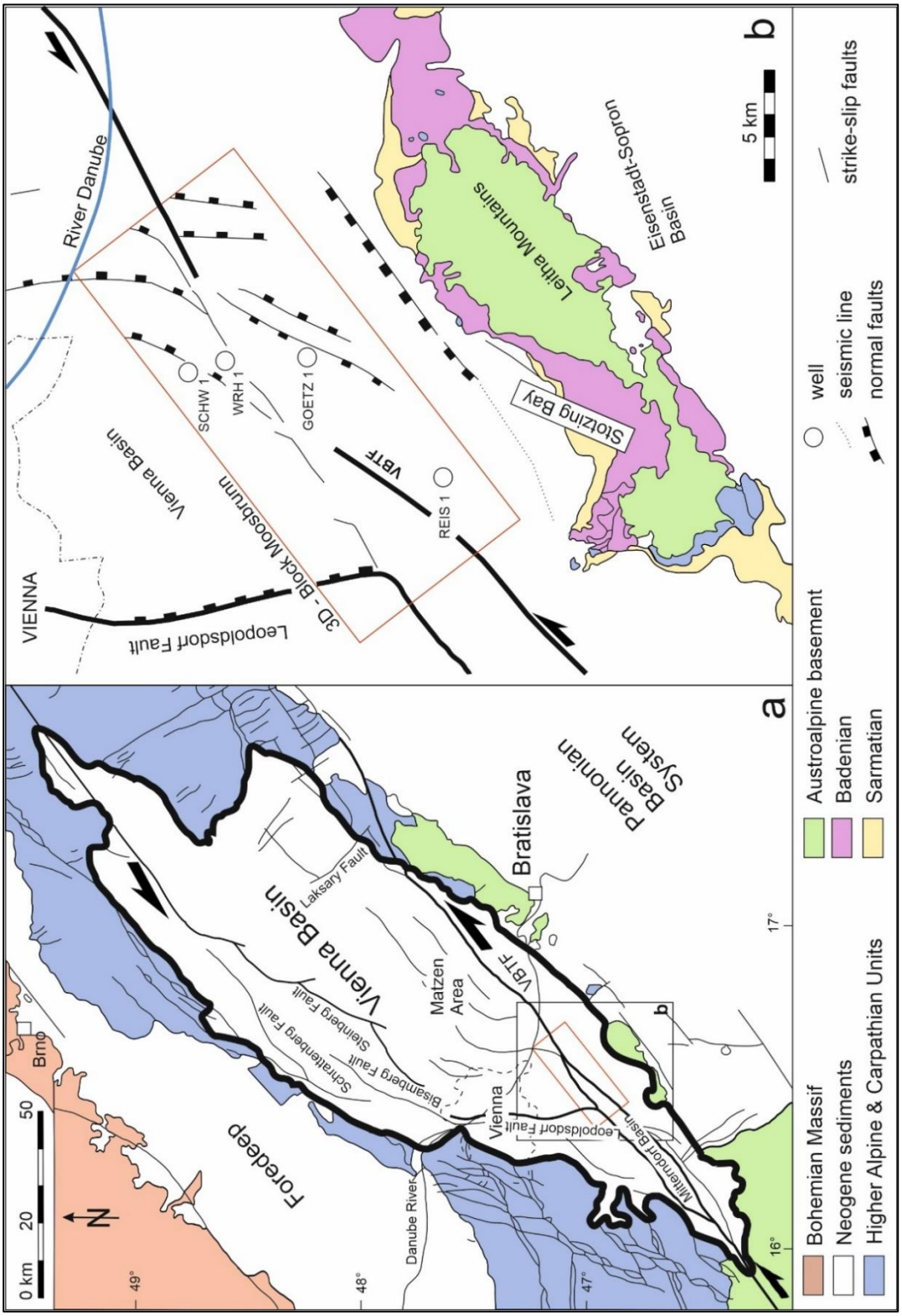

Figure 2: a - Geological setting and structural configuration of the Vienna Basin (modified after Decker et al. 2003 and Strauss et al. 2006). b - Close-up of the position of the 3D- seismic block Moosbrunn (OMV) within the basin showing the main faults and wells used in this study.

2.1 Formation of a piggyback basin in the Lower Miocene

The formation of the Vienna Basin started in the Early Miocene (c. 22-17 Ma) during the final stage of the Alpine-Carpathian-thrusting (Fodor 1995, Decker 1996). The N-S compression of larger parts of the alpine crust led to the development of small east-west trending piggy-back basins on top of the frontal parts of the N-NW propagating thrust belt of the Eastern Alps, which were active from the Eggenburgian up to the Early Karpatian. Lateral paleo-stress fields from the Eggenburgian to Ottnangian indicate a NW-SE compression and led to the development of multiple, lateral displacements (Fodor 2005, Decker et al. 1996, Kováč et al. 2004). Up to the Eggenburgian (c. 17 Ma), the piggy-back basin only extended in the northern part of the Vienna Basin and was characterized by its E-W elongated basin form with an E-W trending basin axis, which is striking oblique to the later forming pull apart-basin and a very low subsidence. The controlling mechanism of those early Miocene basins were ENE-trending sinistral wrench faults, which correlate to faults that were mapped in the most eastern part of the Calcareous Alps (Decker et al. 1996). The resulting basin was active during a period spanning between the Eggenburgian and the Early Karpatian (Decker et al. 1996, Strauss et al 2005).

During the Early Miocene, the sedimentation was closely linked to the opening of small piggy-back basins, which led to a concentrated deposition of Eggenburgian sediments in the most northern part of the Vienna Basin in those newly opened, shallow piggy-back basins. This subsiding sedimentary area was E-W oriented and was a fully marine environment. During the Ottnangian and Early Karpatian, sediments spread to the central parts of the Vienna Basin and it was filled with lacustrine and brackish-lacustrine sediments, which formed parts of the Bockfliess Formation. Those sediments formed small, shallow and E-W trending depressions with less than 500m of thickness. Although thicker depositional packages of up to 800 m can be related to the Bockfliess Formation (Lee & Wagreich et al. 2016). The overlaying Gänserndorf Formation is younger and is represented by lacustrine-terrestrial deposits and a lack of unconformities (Kreutzer et al. 1992). The youngest formation from that period, the Aderklaa Formation, is characterized by limnic-fluvial sandstones, interbedded pelites and fine conglomerates (Weissenbäck et al. 1996) and overlays the older Gänserndorf Formation without major unconformities. A later infill phase during the early Karpatian led to the formation of sediment deposits with a thickness of up to 1000 meters (Lee &

Wagreich et al. 2016). There are no known Eggenburgian sediments from the early Miocene in the southern Vienna Basin.

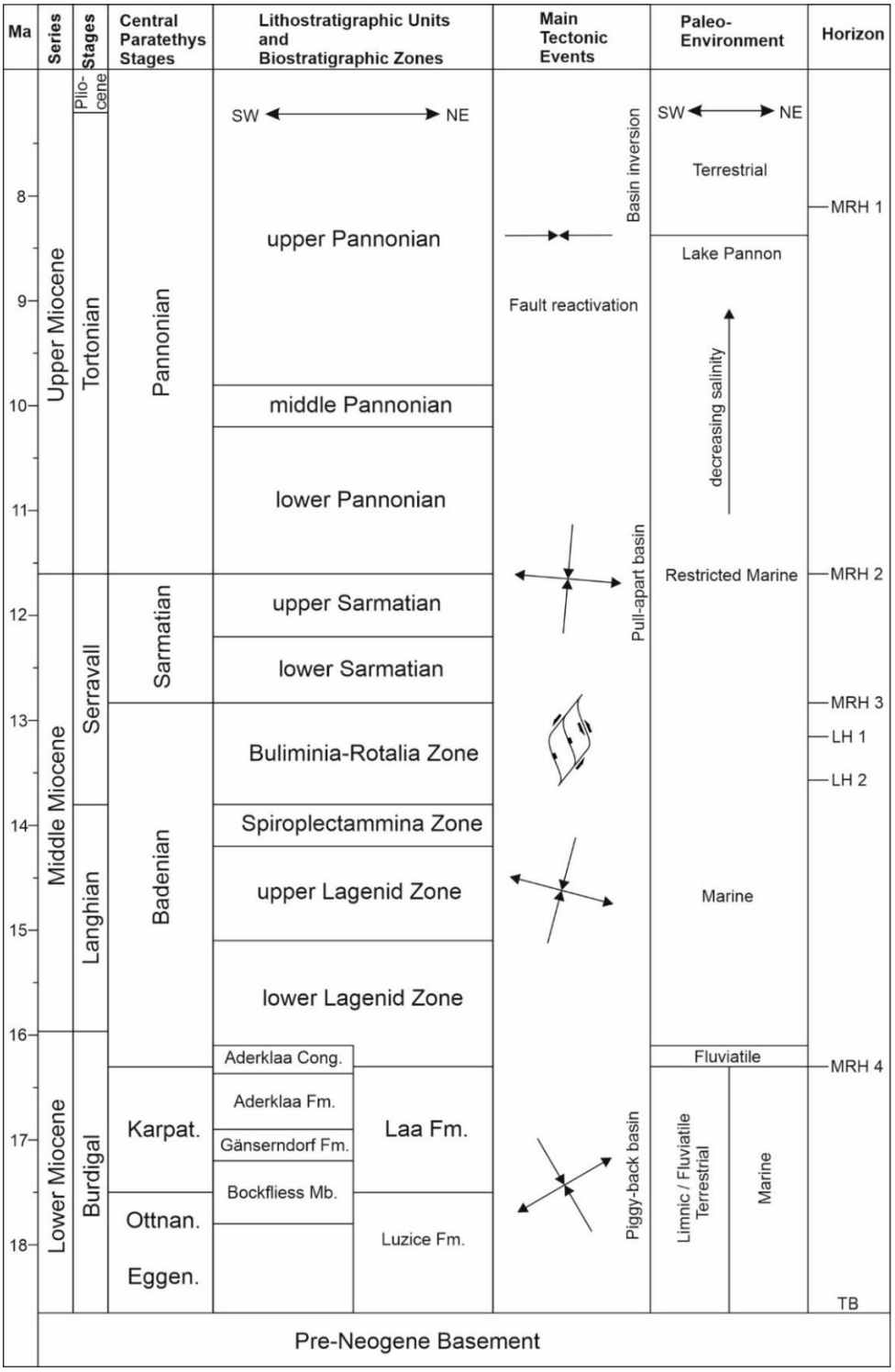

Figure 3: Stratigraphic chart and the structural evolution of the Vienna Basin (modified after Decker 1996; Peresson and Decker 1997; Wagreich and Schmid et al. 2002; Lee and Wagreich et al. 2017).

2.2 Formation of a pull-apart basin from the Middle to Upper Miocene

At the end of the Early Miocene (c 17-16 Ma) the lateral extrusion of the Eastern Alps stopped the thrusting and convergent wrenching of the piggy-back basin structure and led into the evolution of a pull apart structure. During this time, a major basin bounding fault developed in the southeast close to the Leitha Mountains (Wagreich et al. 2002, Hinsch & Decker et al. 2003, Decker et al. 2004, Strauss et al. 2006) and the Vienna Basin gained its present rhombo-shape (Sauer et al. 1992). The N-S compression pushed extruding wedges of the Eastern Alps eastwards between the two NE-striking sinistral faults of the Salzach-Ennstal Fault and the Mur-Mürz Fault and multiple SE-trending dextral faults (Decker et al 1996). The transformation from a piggy-back basin into a pull apart basin happened quickly in less than 1 Ma. The evolution of the basin between the Karpatian and the Pannonian (17 – 8 Ma) was accompanied by an accelerated rift-type subsidence. Two different depocenters formed, one in the northern and one in the southern part of the Vienna Basin and thickness maps show that they reached up to 5.8 km in those 9 Ma (Kröll & Wessely et al. 1993, Decker et al. 1996). The subsidence was controlled by sigmoidal N to NNE trending faults which mostly show normal fault properties and growth data shows that the faulting must have happened synsedimentary during the late Early and Middle Miocene (Kröll & Wessely et al. 1993, Decker et al. 1996, Lee et al. 2015). The northern and southern Vienna Basin both show a general basin asymmetry (Decker et al. 1996). The structures within this newly formed pull-apart basin are dominated by NE-SW trending sinistral strike-slip duplexes and en-echelon listric normal faults with a left stepping geometry. Those NE-SW trending faults reached the platform base of the Bohemian Massif at the western margin of the Vienna Basin during the early Badenian. This activity is indicated by the Steinberg, Schrattenberg and Bulhary faults (Kováč et al. 2004). In the west, the Vienna Basin is bounded by two major syn-sedimentary faults, the Steinberg and the Leopoldsdorfer fault system. Both are Southeast-dipping normal faults and represent (or form) the NW basin margin (Decker et al. 1996). The Steinberg fault with a normal offset of 5.6 km and the Leopoldsdorf fault with a normal offset of 4.2 km along with the Laksary fault, the Farsky fault and the Lanzhot-Hrusky fault (Wessely et al. 1993, Decker et al. 2005), also form the main tectonic elements. The last movements happened around 9 Ma ago in the Pannonian. The delay of movement between the western and eastern part led to the formation of strain and strike-slip faults in the thrust zone. All the characteristics of a pull apart basin can be observed in this

setting, a rhombic basin form and in this case two distinctive depocenters as a direct result of high sedimentation rates in a subsidence zone.

The Vienna Basin changed to a pull-apart basin system controlled by transtension in the late Karpatian. Many Paratethyan nearshore settings indicate the change of the tectonic regime (Wagreich & Schmid et al. 2002) happening at the Karpatian/Badenian boundary and it is documented as a locally major regressive event. The sedimentation during that time is bound by synsedimentary fault blocks and structural ridges (Wagreich & Schmid et al. 2002, Lee & Wagreich et al. 2016). To the south, the sedimentation began discordantly during the Late Karpatian and the Early Badenian. Major depocenters can be located along the Leitha-Lab fault system. This system is made up of strike-slip faults and negative flower structures along the southeastern margin of the basin and between the Steinberg fault and the Laksary fault. Voluminous masses of sediments filled those depocenters. Those sediments were eroded from the Alps and then transported by a developing deltaic system that entered the Vienna Basin from the south (Lee & Wagreich et al. 2016). Sediments that were deposited during the early to middle Badenian usually are up to 500 m thick and confined to the central part of the Vienna Basin. Lower Badenian sediments can be found on multiple stratal units of the Lower Miocene and transgress unconformably. The onlap the northern slope of the Spannberg Ridge, which was later uplifted during the Late Karpatian. Later, during the Late Badenian the area of deposition widens and thickens. The sediments form westward thickening wedges that are bound by synsedimentary faults. The Vienna Basin was mostly influenced by NE-SW and NNE-SSW oriented normal faults and growth strata that developed along those normal faults (Lee & Wagreich et al. 2016). A paleo-Danube delta complex on the western flank of the basin led to thicker sedimentary units. Paleogeographic changes during the middle Badenian led to the development of this delta complex, which carried large amounts of sediment from the Alpine Foreland Basin area into the Vienna Basin.

The Eastern Alps laterally extruded towards the Pannonian area in the east. This extrusion resulted in complex strike-slip faulting and back-arc extensions, which led to the development of pull-apart basins like the Vienna Basin in the Miocene.

2.3 East-west compression and basin inversion from the Upper Miocene into the Pliocene

Overprinting microtectonic structures in the Vienna Basin show an E-W shortening as one of the most recent tectonic events. During that event, Early and Middle Miocene faults were reactivated. The strain of that E-W shortening dextral offset cannot be quantified exactly but it seems to be very low compared to the strain of earlier tectonic phases. The E-W compression can be dated to the late Pannonian (9 to 5,6 Ma) and correlates with the age of the youngest deposits in the Vienna Basin. Those deposits are Pannonian lithostratigraphic units. There are no known significant volumes of sediments in the Vienna Basin that are younger than Pannonian. The only exception are local fluviatile gravels that are of Pontian age and unconformably overlay the Pannonian sediments. The E-W compressive stress field evolved and led to the basin inversion uplift of more than 200 m (Lee et al. 2015) of the Vienna Basin and sediment deformation and erosion in it (Lee & Wagreich et al. 2016). The basin inversion during the Pliocene is documented by fault-controlled subsidence of Grabensystems at the eastern margin of the Vienna Basin (Kováč et al. 2004). Substantial post-Pannonian surface uplift at the margin and in the northern part of the Vienna Basin is indicated by Neogene marine deposits cropping out to a maximum topographic height between 300 to 400 m (Decker et al. 1996). This event must have taken place in the last 8 Ma, but the uplifted Sarmatian sediments and brackish Pannonian sediments only give loose time constraints (Decker et al. 1996). It is clear that the surface uplift must have been at least 300 m, as the sea level in the Mediterranean region during the Early Pannonian was around 50m above the recent sea level (Decker et al. 1996).

2.4 East-west directed extension lasting from the Pleistocene up to recent

A sinistral transtensional regime led to fault-controlled subsidence resulting in recent seismic activity along the eastern and south-eastern border of the Vienna Basin. The fault zones are a prolongation of the seismically active zones in the Eastern Alps and the Western Carpathians (Gutdeutsch and Aric 1988). This reactivation of the Vienna basin is linked to the NE-SW extension at releasing bends of Pleistocene Basins like the Mitterndorf or Aderklaa basins since 300 - 200 Ka (Salcher et al. 2012).

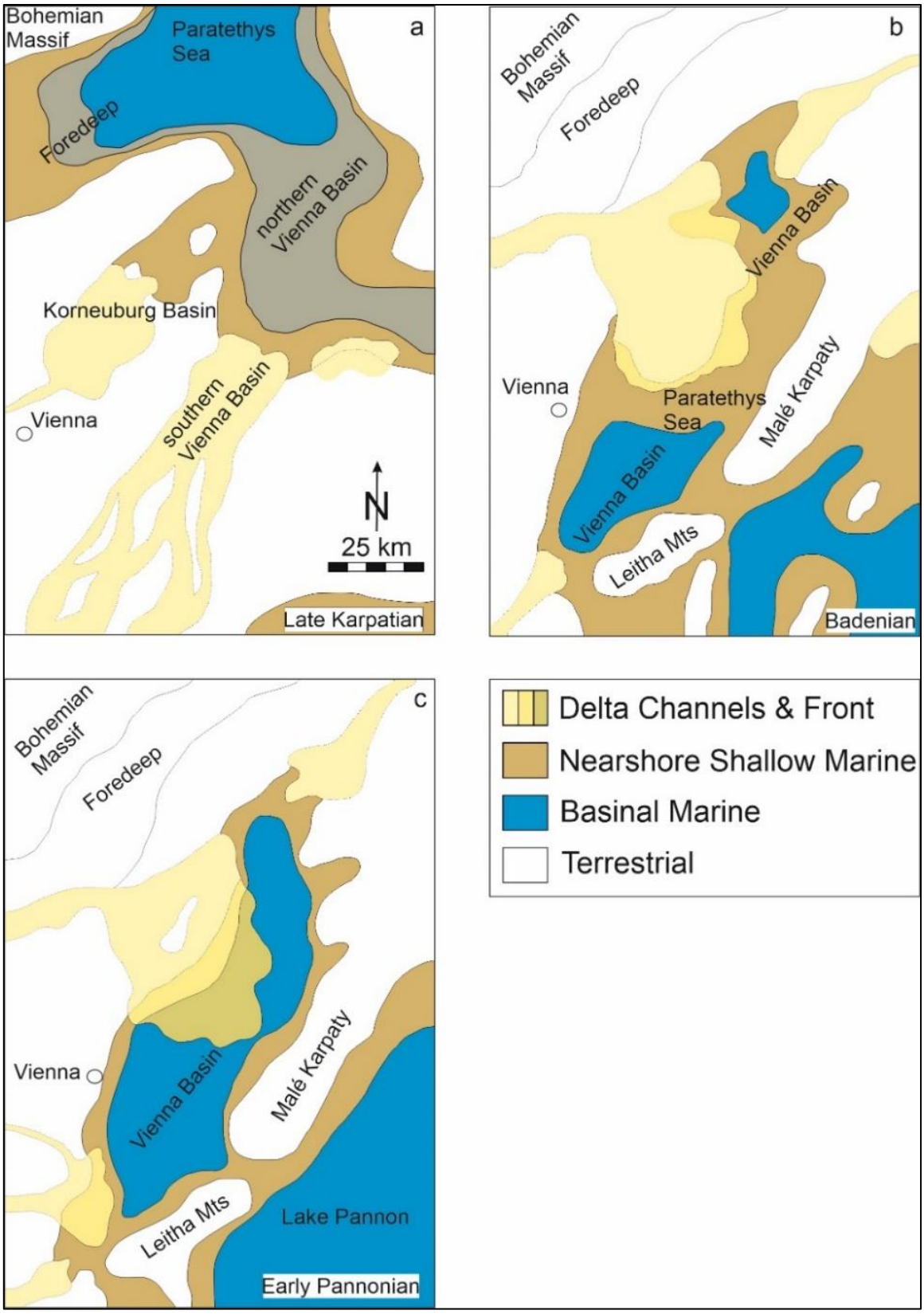

Figure 4: Simplified paleogeographic maps showing the Miocene evolution of the Vienna Basin at three stages: **a** –during Late Karpatian, **b** – during Badenian, **c** –during Early Pannonian times. Modified after Sauer et al. 1992; Kováč et al. 2004; Strauss et al. 2006.

This extension takes place at a releasing bend along the multiple slow moving sinistral strike-slip faults (1-2 mm/year) along the Vienna Basin transfer Fault (VBTF; Decker et al. 2005). The most recent stress and focal mechanisms show sinistral strike-slip faulting along the north-east striking subvertical faults (Hinsch et al. 2005b). Today, it is unclear if the present kinematics of the fault system represent a pull-apart system or a linear strike-slip fault at the southern border of the Vienna Basin.

Small younger Quaternary basins are mostly filled with fluvial sediments of up to 150m and unconformably overlying Miocene sediments (Decker et al. 2005, Hinsch et al. 2005b, c, Salcher et al. 2012, Lee & Wagreich et al. 2016). North of the Danube, those basins are filled with coarse gravels and overbank fines of the Danube that overlay the mostly marine Neogene sediments unconformable. In the south the basins are filled with sediments derived from Alpine catchments and show a distinct cyclicity of thick sequences of coarse sediments that were deposited during cold periods and thin sequences of channel and flood sediments that were deposited during warmer periods (Salcher et al. 2012).

Chapter 3: Data and Methodology

3.1 Database

This study used the 3D reflection seismic survey Moosbrunn (Figure 5) that covers the southern part of the Vienna Basin. The 3D seismic data is complemented with 2D seismic lines and well data (Figure 5, Table 1), all of which were kindly provided by OMV Vienna. The wells are correlated to the seismic survey by velocity information from checkshot surveys and velocity functions (e.g., 1s TWT (Two Way Time) corresponds to 1100m depth, 2 s TWT to 2600m and 2.2 s TWT to approx. 3000 m (Strauss et al. 2006). Four wells that are located inside the 3D seismic block include Goetzendorf 1 (GOETZ 1), Reisenberg 1 (REIS 1), Schwadorf 1 (SCHW 1) and Wienerherberg 1 (WRH 1) and were primarily used for seismic mapping (Figure 2; Table 1).

The seismic stratigraphic framework used in this thesis follows the methodology and terminology of Vail et al. (1977) and Mitchum et al. (1977). The reflexions configuration, bounding relationships and external geometry led to the identification of different seismic packages.

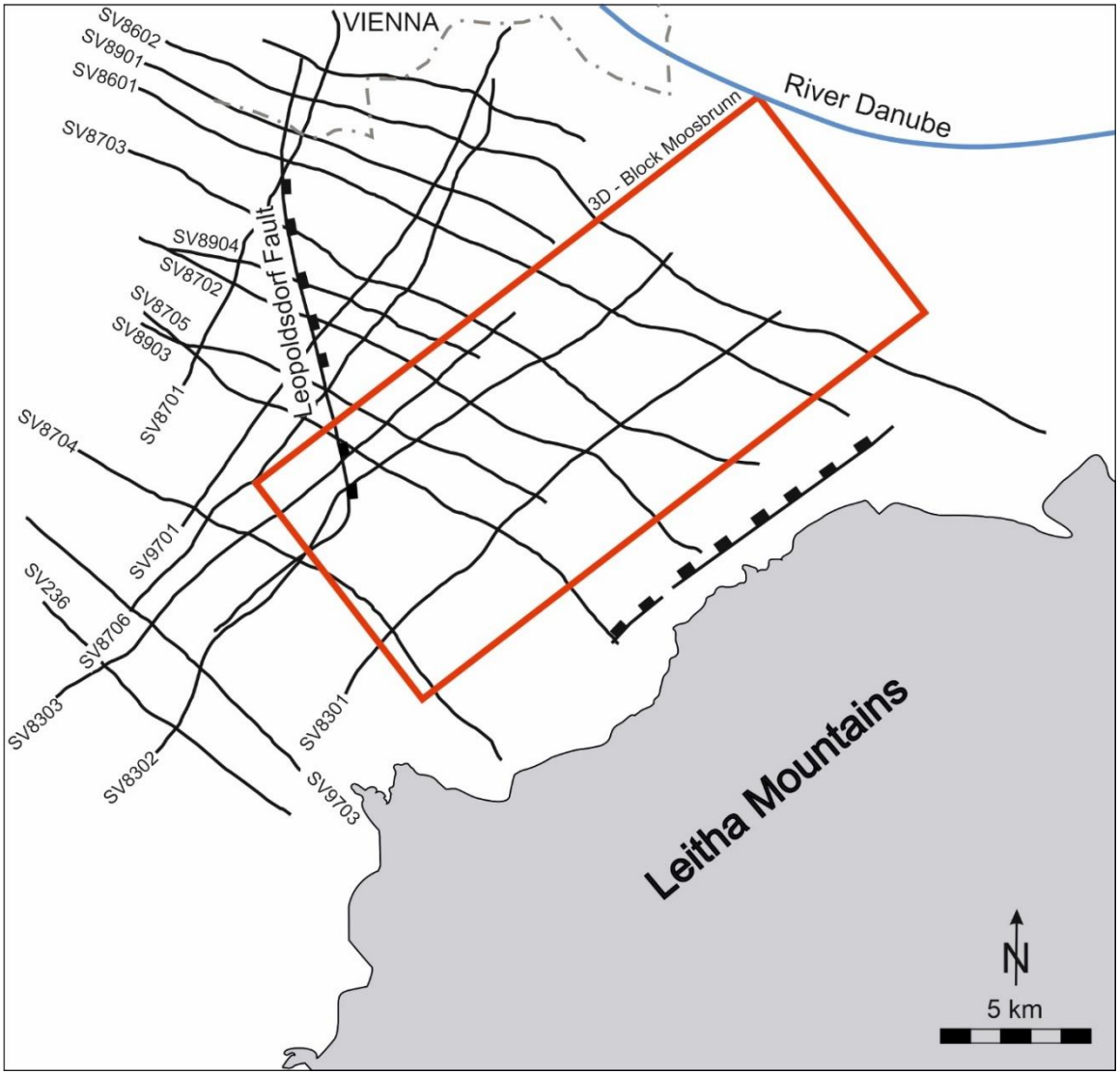

Figure 5: Sketch of 2D Lines and the position of the 3D Cube Moosbrunn (OMV).

3.2 Setting of the 3D seismic block

The 3D seismic cube shown in Figure 5 has a crossline length of 9050 m and an inline length of 21624 m. The seismic data provided are time-migrated with a maximum depth of 4000 ms (TWT). Generally, the interpretability of the data is good, although there are significant differences in the quality and seismic resolution throughout the seismic cube. Namely, the northern part of the 3D cube is characterised by lower data quality, when compared to the rest of the seismic survey. Also, the seismic resolution decreases rapidly with an increasing depth. Large-scale faults can be traced down to c. 3000 ms TWT and most of the horizons and smaller faults down to a depth of c. 2250 ms TWT. The quality of the 2D seismic lines is generally lower, but it still allows to interpret large-scale faults and to tie those into the structures identified on the 3D

seismic data. Vertically, seismic features on 2D lines can be identified down to c. 3000 ms at maximum. The length of the used 2D lines varies from 10 to almost 30 km.

Number	Well Name	Abbreviation	Depth (m)
1	Goetzendorf 001	GOETZ 1	2240 m
2	Reisenberg 001	REIS 1	1140 m
3	Schwadorf 001	SCHW 1	1210 m
4	Wienerherberg 001	WRH 1	2400 m

Table 1: List of used wells inside the 3D-Cube Moosbrunn (OMV). (Location of wells see Fig. 2b).

3.3 Methodology

Petrel 2018 software, kindly donated by Schlumberger, was used for seismic interpretation in this study. During the initial stage of seismic interpretation of the 3D-Block Moosbrunn, faults and horizons were mapped manually on every 5th crossline and inline in order to get a detailed geometry and lateral extent of individual seismic features. Later, 2D seismic lines were interpreted and integrated to the 3D seismic survey, where possible (e.g., Figure 6a). As a next step, the derived 3D horizon maps were processed using the autotracking tool in Petrel (basic 3x3) to fill the grid and get a seismic interpretation in areas otherwise difficult to pick (e.g., Figure 6b). Lastly, the surface maps and time thickness maps were generated using Petrel software to visualize individual Miocene depocentres and maximum thicknesses within individual seismic packages. The last step was done for both 2D and 3D seismic data, and it resulted in maps covering much larger areas (e.g. Figure 6c). It is noted that the resolution in the area covered by 2D lines is lower than in the 3D cube.

Chapter 4: Results

4.1 Introduction

This chapter addresses the regional seismic architecture of the southernmost part of the Vienna Basin and presents new findings regarding Miocene fault activity, and distribution and thicknesses of individual Miocene seismic packages. The packages are defined by four main regional and three local seismic horizons, interpreted based on their seismic appearance. Karpatian, Badenian, Sarmatian and Pannonian horizons are the four main regional horizons, and Intra-Badenian Top, Intra Badenian Bottom and pre-Neogene Basement are the three local horizons (Table 2; Figure 3). Based on this study, the thickness of the Miocene strata is at least 1750 ms TWT.

Section 4.2 gives an overview of the newly interpreted seismic horizons while section 4.3 introduces the seismic packages, including the quality of the seismic data, the thickness and character of the seismic facies. It also includes time-thickness maps of the three uppermost seismic packages (Badenian, Sarmatian and Pannonian) and includes the evolution of individual depocenters, i.e., a depocenter shift from the north during the Karpatian to the south during the Pannonian. Section 4.4 addresses the basin's structural setting, which includes four newly interpreted main fault groups with different fault orientations, locations and sizes. Section 4.5 gives an overview of the 2D data as well as the main features and structures interpreted on the lines.

4.2 Seismic horizons

Manual seismic interpretation resulted in the definition of four regionally mapped seismic horizons: (i) Karpatian, (ii) Badenian, (iii) Sarmatian and (iv) Pannonian (Table 2; Figure 3 & 6) and three locally mapped horizons (v) Intra-Badenian Top, (vi) Intra Badenian Bottom and (vii) and pre-Neogene Basement. All horizons are listed in Table 2 and shown in Figure 7. Based on this study, the minimum estimated thickness of the Miocene strata is at least 1750 ms TWT.

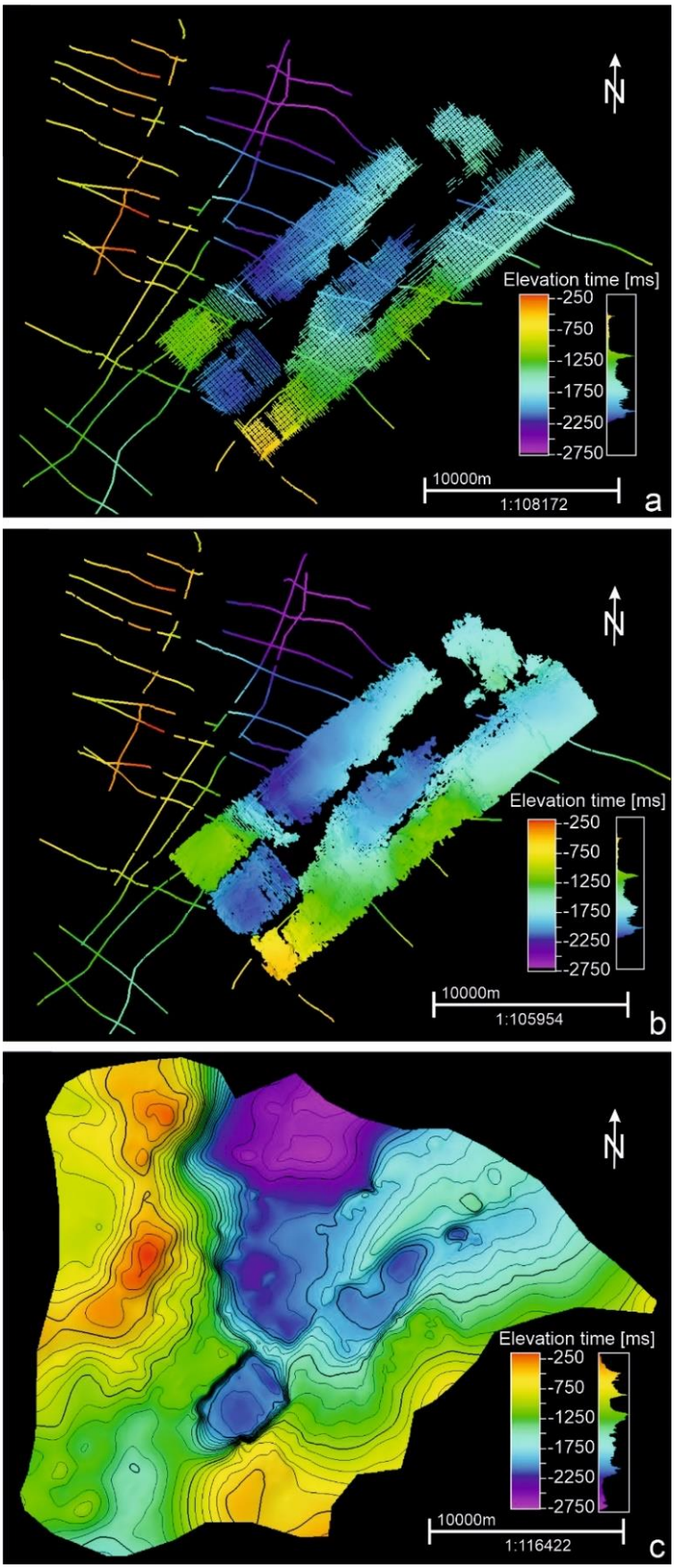

Figure 6: Seismic horizon MRH 4 (Karpatian); (a) – Manually picked seismic horizons (2D & 3D), (b) – seismic horizon auto tracked (3x3) (3D), (c) – seismic surface created from seismic horizon map (2D & 3D)

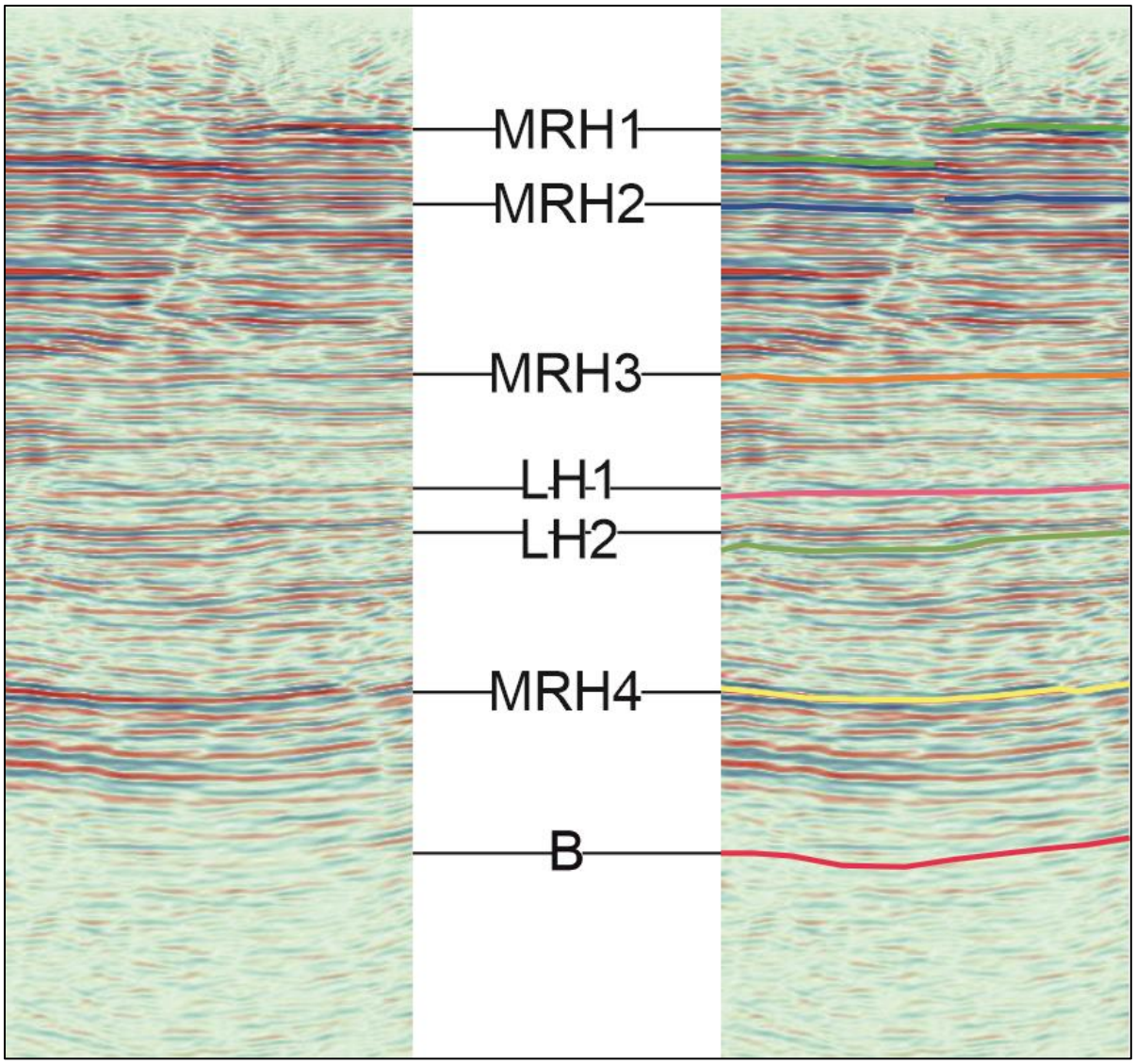

Figure 7: Interpreted regional and local seismic horizons with their seismic character shown.

Seismic horizon MRH4 – Karpatian

Seismic horizon MRH4 can be traced with confidence throughout the entire 3D seismic cube, except for the deepest parts of the central graben, where the seismic resolution and the absence of strong reflectors do not permit seismic picking with high confidence (Figure 6a). In general, the interpreted horizon represents a high-amplitude, laterally prevalent seismic reflector, which marks the top of the Karpatian strata and the base of the Badenian sedimentary succession (Figure 7). It was picked as a negative amplitude. The Karpatian horizon MRH4 is a very prominent seismic reflector also in the case of 2D seismic lines. However, along these lines the horizon represents the deepest picked horizon because the seismic section below usually does not have coherent character and does not contain any significant laterally extensive reflectors.

Main Regional Horizons	Age	Colour (in Petrel)
MRH 1	Pannonian	Green
MRH2	Sarmatian	Blue
MRH3	Badenian	Orange
MRH4	Karpatian	Yellow
Local Horizons	**Age**	**Colour**
LH1	Intra Badenian Top	Pink
LH2	Intra Badenian Bottom	Grey
B	Pre-Neogene Basement	Red

Table 2: List of interpreted regional and local horizons on the 2D Lines and inside the 3D Cube Moosbrunn (OMV).

Seismic horizon MRH3 – Badenian

Seismic horizon MRH3 can be traced throughout the entire 3D seismic cube, except for the NW corner and to a smaller degree inside the main central graben system due to poor seismic resolution, which does not allow an accurate interpretation (Figure 8). In those deeper parts, the lack of high-amplitude reflectors and insufficient well control makes it difficult to pick the position of horizon MRH3. In shallower areas, however, the horizon represents a medium to high amplitude seismic reflector that defines the top of the Badenian succession (Figure 7). The horizon was picked as a negative amplitude in the 3D cube. Along the 2D seismic lines, the horizon is not picked in the westernmost segment (Figure 8a) and it has variable seismic character ranging from low to medium amplitude.

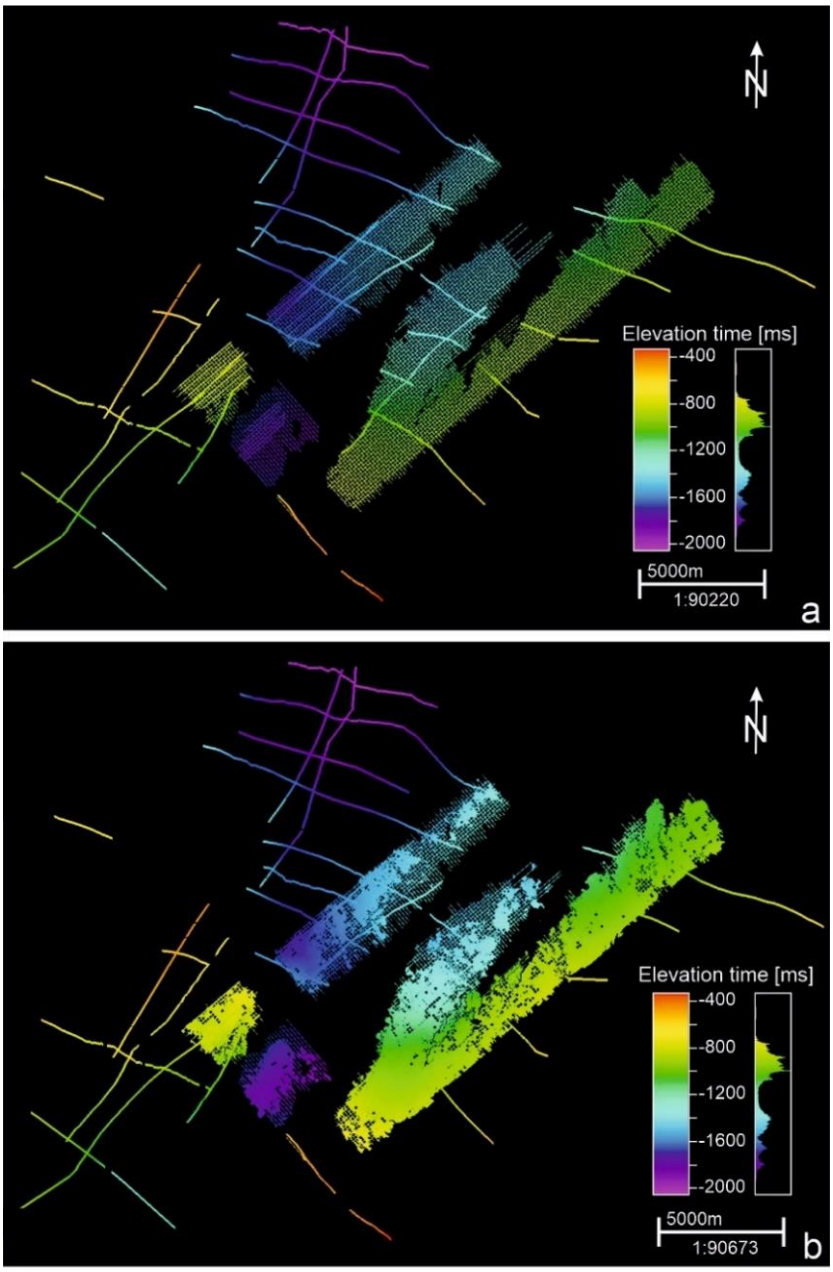

Figure 8: Seismic horizon MRH 3 (Badenian); (a) – Manually picked seismic horizons (2D & 3D), (b) – seismic horizon auto tracked (3x3) (3D), (c) – seismic surface created from seismic horizon map (2D & 3D)

Seismic horizon MRH2 – Sarmatian

This interpreted seismic horizon covers the smallest area in the 3D seismic cube as well as along the 2D lines, when compared to the other horizons described here (Figure 9). Seismic horizon MRH2 defines the top of Sarmatian succession and is traced with confidence throughout most of the shallower parts of the 3D seismic cube, with the exception of the NW corner and also certain areas in the deeper central graben system. Poorly visible and diffuse seismic reflectors in those areas, together with lack of well control, do not allow any detailed interpretation of horizon MRH2. In shallower areas of the 3D cube, the horizon represents high amplitude, mostly laterally prevalent seismic reflectors (Figure 7). The amplitude was picked as a negative. Along the 2D lines, the horizon has medium amplitude character but locally represents high amplitude laterally prevalent seismic reflector.

Seismic horizon MRH1 – Pannonian

The youngest seismic horizon MRH1 is traced throughout the entire 3D seismic cube owing to its shallowest position and good quality of the data (Figure 10). Yet, to a small degree, interpretation in the NW corner and within the central graben system was carried out with some uncertainties due to a significant increase in depth in the central area and a related decrease of seismic resolution. Horizon MRH1 defines the top of the Pannonian succession. On 3D seismic, the horizon was picked along high amplitude seismic reflector in areas surrounding the central graben system (Figure 7), which is contrasting with its generally low to very low amplitude character of seismic reflectors and poorly reflective appearance. The amplitude was picked as a negative. On 2D data, the horizon is also represented by high-amplitude seismic reflectors elsewhere, but the amplitude decreases abruptly in the central graben system.

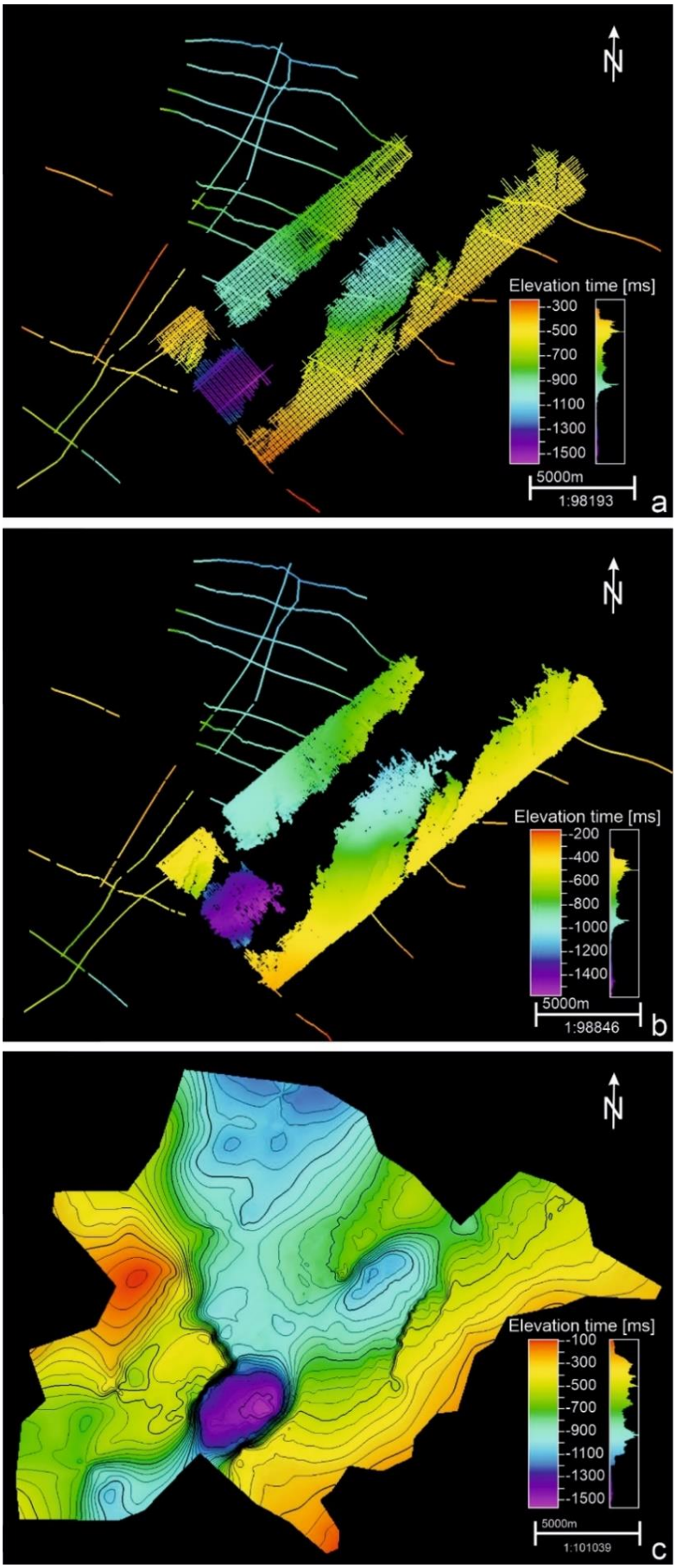

Figure 9: Seismic horizon MRH 2 (Sarmatian); (a) – Manually picked seismic horizons (2D & 3D), (b) – seismic horizon auto tracked (3D), (c) – seismic surface created from seismic horizon map (2D & 3D)

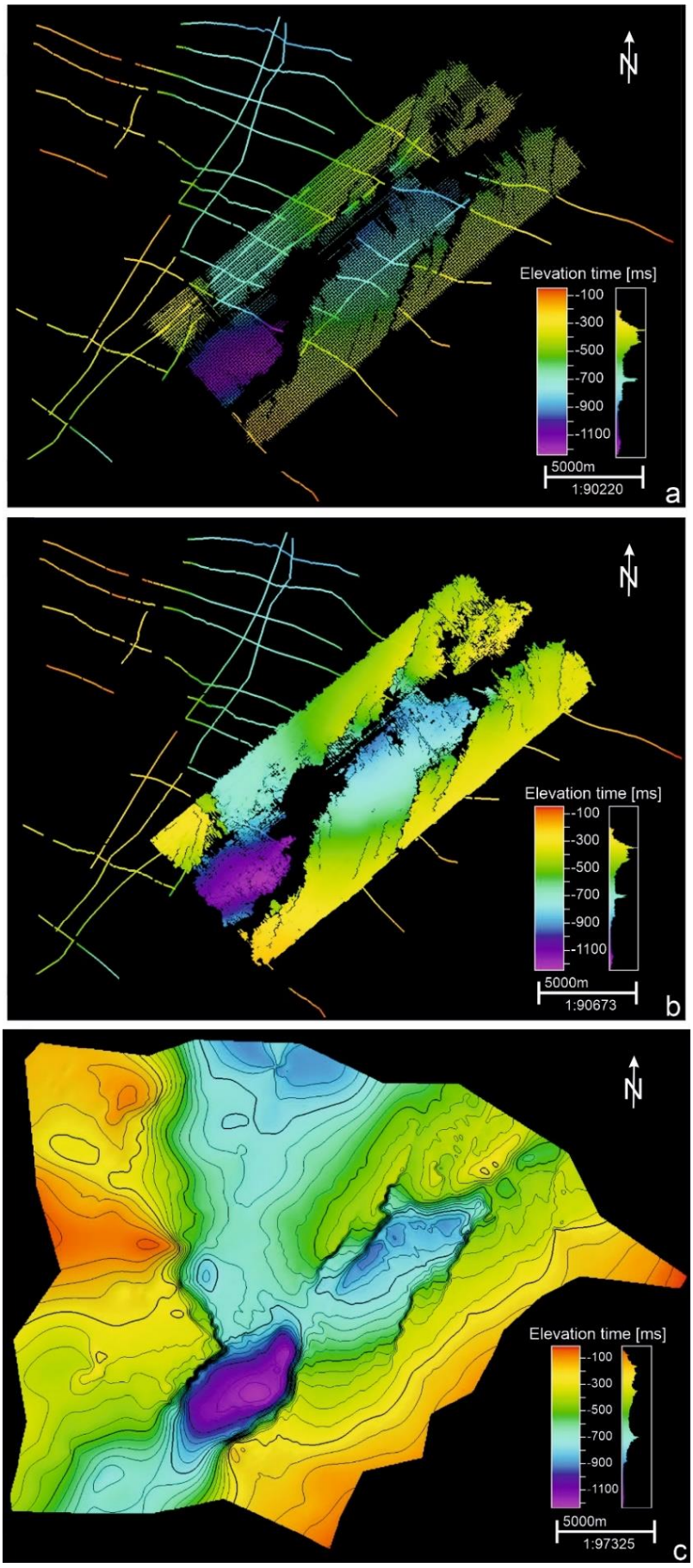

Figure 10: Seismic horizon MRH 1 (Pannonian); (a) – Manually picked seismic horizons (2D & 3D), (b) – seismic horizon auto tracked (3x3) (3D), (c) – seismic surface created from seismic horizon map (2D & 3D)

Seismic horizon B – pre-Neogene basement

Seismic horizon B and the two following horizons have only local significance and are therefore described only briefly here. Horizon B is only interpreted in the NE part of the 3D seismic cube and is not defined on any of the 2D lines. Where present, it predominantly has a low amplitude character and is interpreted to define the probable base of the Karpatian sedimentary succession (Figure 7). However, it is possible that it might represent intra-Karpatian seismic reflector due to no well control in the area.

Seismic horizons LH1 and LH2

These two horizons of local significance were picked in the NE part of the seismic cube. Both of them represent medium amplitude, laterally prevalent seismic reflectors (Figure 7) and they are both interpreted to occur within the Badenian sedimentary succession. They were picked along negative amplitudes.

4.3 Seismic packages

In this section, a brief overview of six interpreted seismic packages is given. Four of them have been picked throughout the entire 3D seismic cube and also on the 2D data. Three packages defined between the two inter-Baden horizons and the Basement seismic package occur only in the NE part of the 3D cube. Seismic characteristics of each package is given in Table 3.

In general, all of the packages can be interpreted with high confidence except for the central NE-SW trending graben system. There the seismic resolution is significantly decreased due to intense faulting and possibly other aspects, which however are not pursued in this study.

Seismic Sequence	Thickness (ms TWT)	Character of seismic facies	Bounding Horizons
Pannonian (Pan)	100 - 400	Good seismic resolution mostly continuous and parallel seismic reflectors high amplitude reflectors are common	MRH1 – MRH2
Sarmatian (Sar)	100 – 900	High amplitude, generally laterally prevalent reflectors, some areas are of low resolution with a chaotic appearance	MRH2 – MRH3
Intra Badenian (i.Bad)	50 – 200	High to medium amplitude seismic reflectors, laterally restricted. Low seismic resolution due to massive faulting in the main fault zone.	LH1 – LH2
Badenian (Bad)	200 – 1000	Medium to high amplitude seismic reflectors, parallel to sub-parallel reflectors occurs in the NE part of the 3D cube	MRH3 – MRH4
Karpatian (Kar)	0 - 800	Top well defined in few parts of seismic, basement and lower boundary with low resolution and not well defined, sometimes no boundary between Kar and top of B, parallel and divergent seismic reflectors	MRH4 - B
Basement (B)	Minimum thickness of 4000	Low seismic resolution, seismically transparent to low amplitude discontinuous reflectors Top of package only visible in the NE part of the 3D cube, the base of this package is not defined	Horizons B or MHR4 define the top of the package, the base of this package is not defined.

Table 3: List of interpreted seismic packages and their description. For abbreviations of seismic horizons see Table 2.

Seismic package 1 – Basement (B)

The top of the basement package is defined by the oldest interpreted horizon B in the NE part of the 3D seismic cube (Figures 7, 11 and 12). In the rest of the study area, the top of the basement package is not interpreted, but in some areas, it is defined by horizon MRH4, i.e., along the 2D lines and in a larger part of the 3D seismic cube (Figure 11), and it is directly overlain by the Badenian package. The top of the basement package was encountered in wells Goetzendorf 1 (GOETZ 1) and Wienerherrberg 1 (WRH 1) (see Table 1). On the other hand, the base of this package is not defined due to generally low seismic resolution, lack of laterally prevalent reflectors and overall chaotic seismic appearance. Most faults cannot be interpreted deeper into the basement package, but they clearly offset the top of the package. Maximum thickness of this package is not estimated.

Seismic Package 2 – Karpatian (Kar)

The Karpatian package is interpreted to occur between horizons B and MRH4 (Figures 7 and 11) and can only be interpreted with certainty in the NE part of the 3D seismic cube. The top of the Karpatian package is mostly well defined by strong seismic reflector, while the lower boundary is characterized by mostly low amplitude seismic reflector (horizon B). Seismic reflectors close to the top of the package show parallel geometry and larger lateral continuity, while the lower half of the package lacks any consistent reflectors and has low amplitude seismically transparent character. Its thickness varies strongly and reaches a maximum thickness of up to 700 ms TWT. The seismic stratigraphy is based on wells that are shown in Table 1. There is one major fault, EFG-16 that defines the western limit of this package, seismic reflectors onlap the fault EFG-16 and the entire package exhibits stratal thickening towards the northeast (Figure 11).

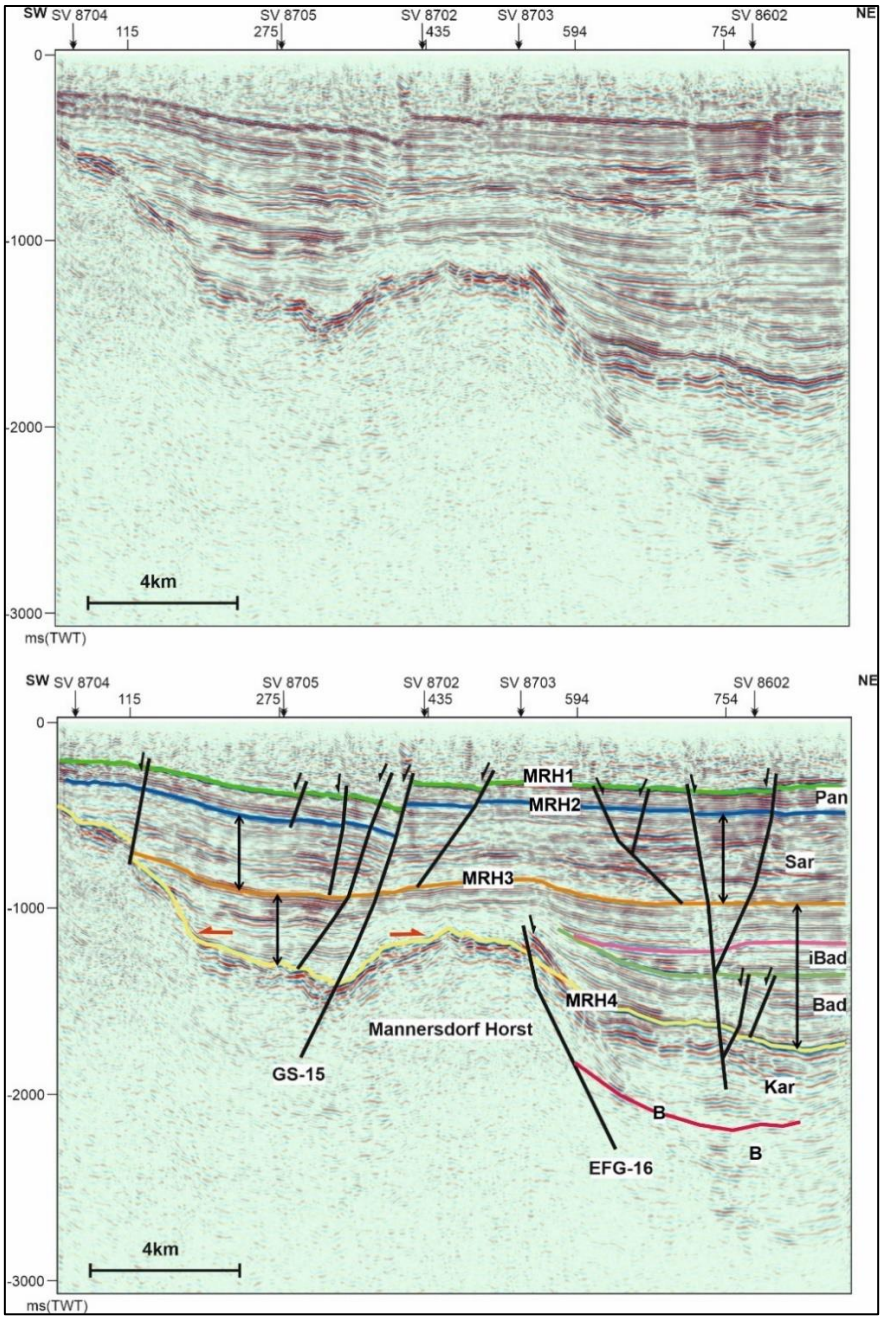

Figure 11: Seismic line IL 87 showing the four main packages as well as the basement and the intra-Badenian local packages. Significant thickening of the Badenian package (shown by black arrows) is observed across NW-SE trending fault EFG-16. This fault constrains the southern limit of the Karpatian package. The Graben System fault GS-15 with a NE-SW strike, dominates the SW part of the seismic line. Small onlaps within the Badenian package are indicated by the red arrows. Horizons: B-Basement, MRH4 – Karpatian, MRH3 – Badenian, MRH2 – Sarmatian, MRH1 – Pannonian. Packages: B – Basement, Kar – Karpatian, iBad – Intra Badenian, Bad – Badenian, Sar – Sarmatian, Pan – Pannonian. For location see Figure 12.

Seismic package 3 – Badenian (Bad)

The Badenian package is interpreted between horizons MRH4 and MRH3 (Figures 7 and 11). It is encountered in wells Wienerherrberg 1 (WRH 1 in Figure 2b and Table 1). When compared to older Karpatian package, this package is seismically much better stratified. It contains laterally continuous medium to high amplitude seismic reflectors with variable geometries, e.g., sub-parallel to divergent. Its thickness varies throughout the cube and reaches more than 800 ms TWT, with the thickest successions in the NE (Figure 14). The most prominent feature within this package is the Intra-Badenian sub-package and is described separately below. In the SW, the Badenian package exhibits onlaps on the existing palaeotopography (shown by red arrows in Figure 11).

Seismic package 4 – Intra Badenian (iBad)

The Intra-Badenian package is only found in the NE part of the 3-D block and is defined between the local horizons LH1 and LH2 (Figure 7 and 11). It shows continual stratal thickening towards the NE (up to 200 ms TWT thick) and is characterized by a medium to high resolution laterally continuous seismic reflectors. It is pinching out towards the central basement high, which is delimited by fault EFG-16. Internally, onlaps are seen within this package.

Seismic Package 5 – Sarmatian (Sar)

The overlying Sarmatian package is interpreted between horizon MRH3 and MRH2 (Figures 7 and 11) and is characterized by high amplitude laterally continuous seismic reflectors with local areas, which exhibit loss of coherent structure due to presence of faults (Figure 13). The package was encountered in well Reisenberg 1 (REIS 1, see Figure 2b and Table 1). Its thickness varies largely between 100 and 900 ms TWT, reaching the maximum thickness in the northern part of the study area (Figure 15). In some areas, the package exhibits stratigraphic onlaps on to the adjacent basement high (Figure 11).

Seismic Package 6 – Pannonian (Pan)

The youngest Pannonian package is defined between horizons MRH2 and MRH1 and exhibits predominantly parallel and laterally continuous seismic reflectors of high to low amplitudes (Figures 7 and 11). There are areas of lower seismic resolution, however, they occur within fault zones. The seismic package exhibits generally lower resolution and reflectors with lower amplitude towards to the top. The package is encountered in well Reisenberg 1 (Figure 2b and Table 1). The thickness of the Pannonian varies between 100 and 450ms TWT (Figure 16).

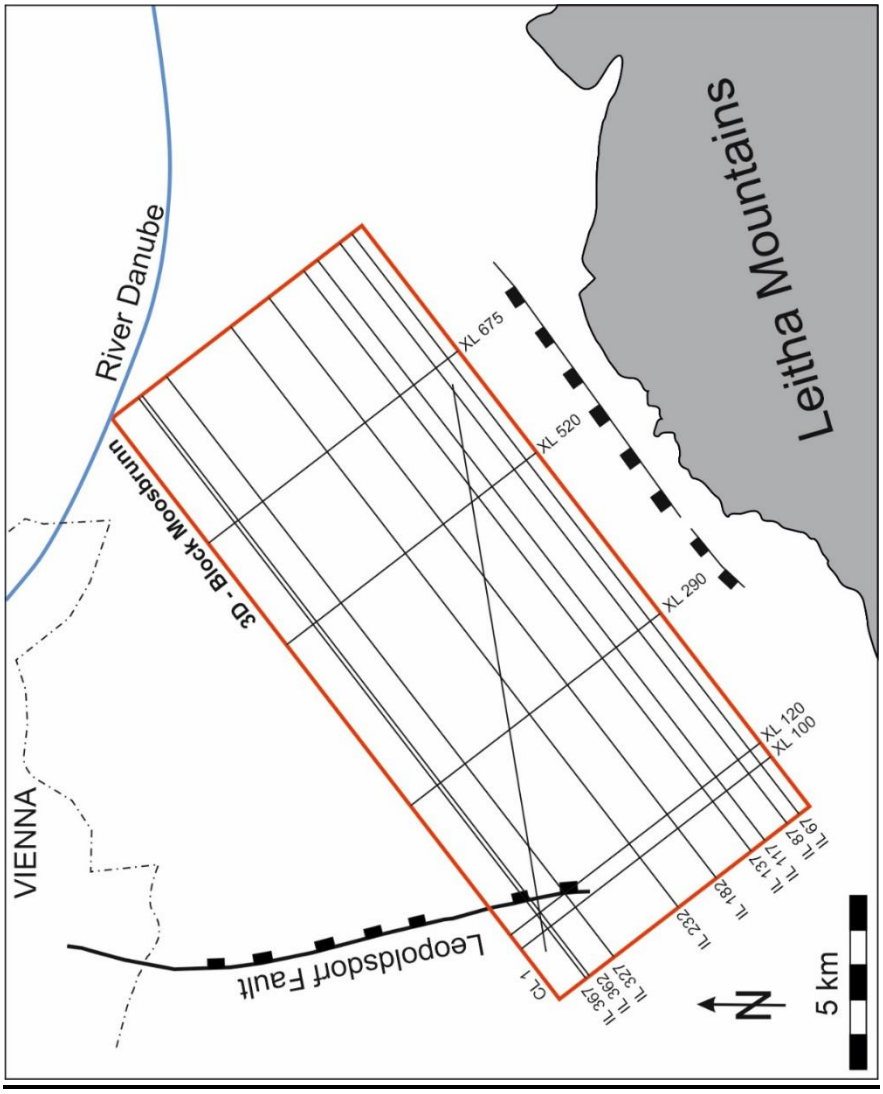

Figure 12: Location of 3D lines shown in this study, including one composite line (CL1).

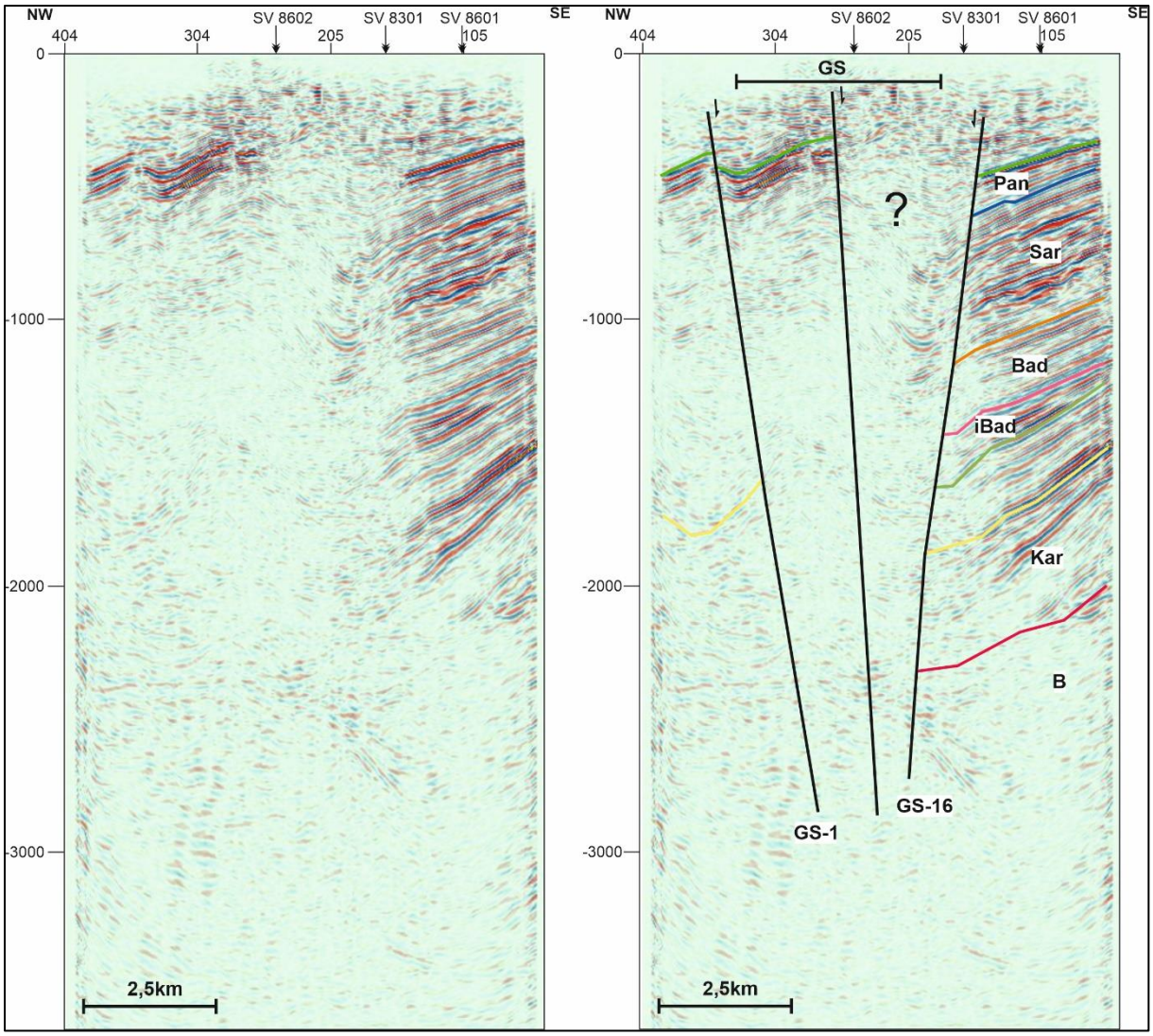

Figure 13: Seismic line XL 675 showing the interpreted seismic packages. The poor quality of seismic data, low resolution and loss of coherent seismic reflectors is typical for the central part of the seismic cube, i.e., within the major fault zone (GS), preventing detailed interpretation of the horizons (shown by question mark). The three normal faults with a NE-SW strike are part of the Graben System (GS) and can be interpreted down to a depth of c. 3000 ms TWT. For abbreviations see Figure 11. For location see Figure 12.

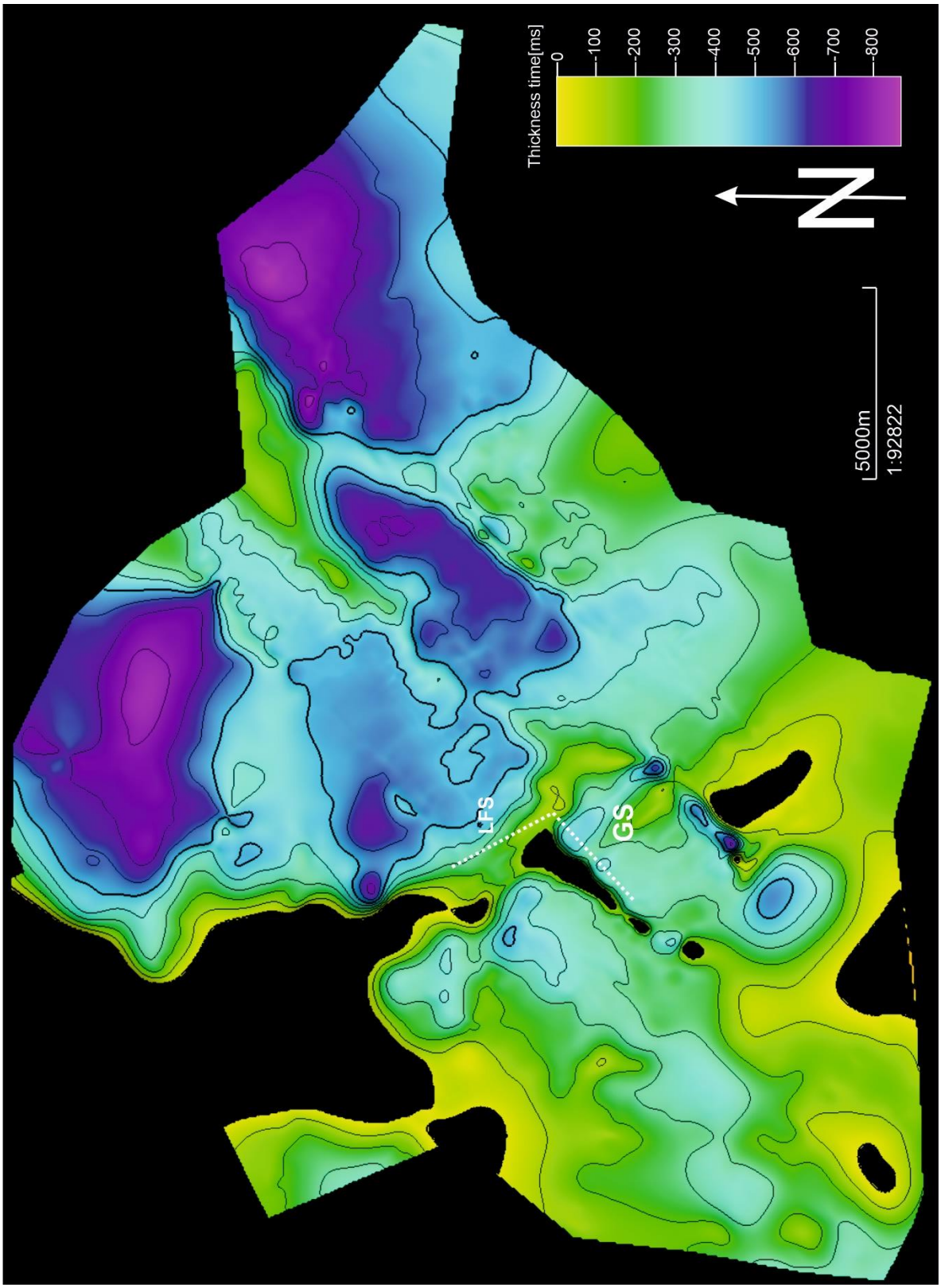

Figure 14: Thickness map of the Badenian package. Maximum thickness of the package is more than 800 ms. Figures 14-16: black areas on the maps represent faults or places, where one of the two surfaces is not interpreted (due to the low seismic resolution).

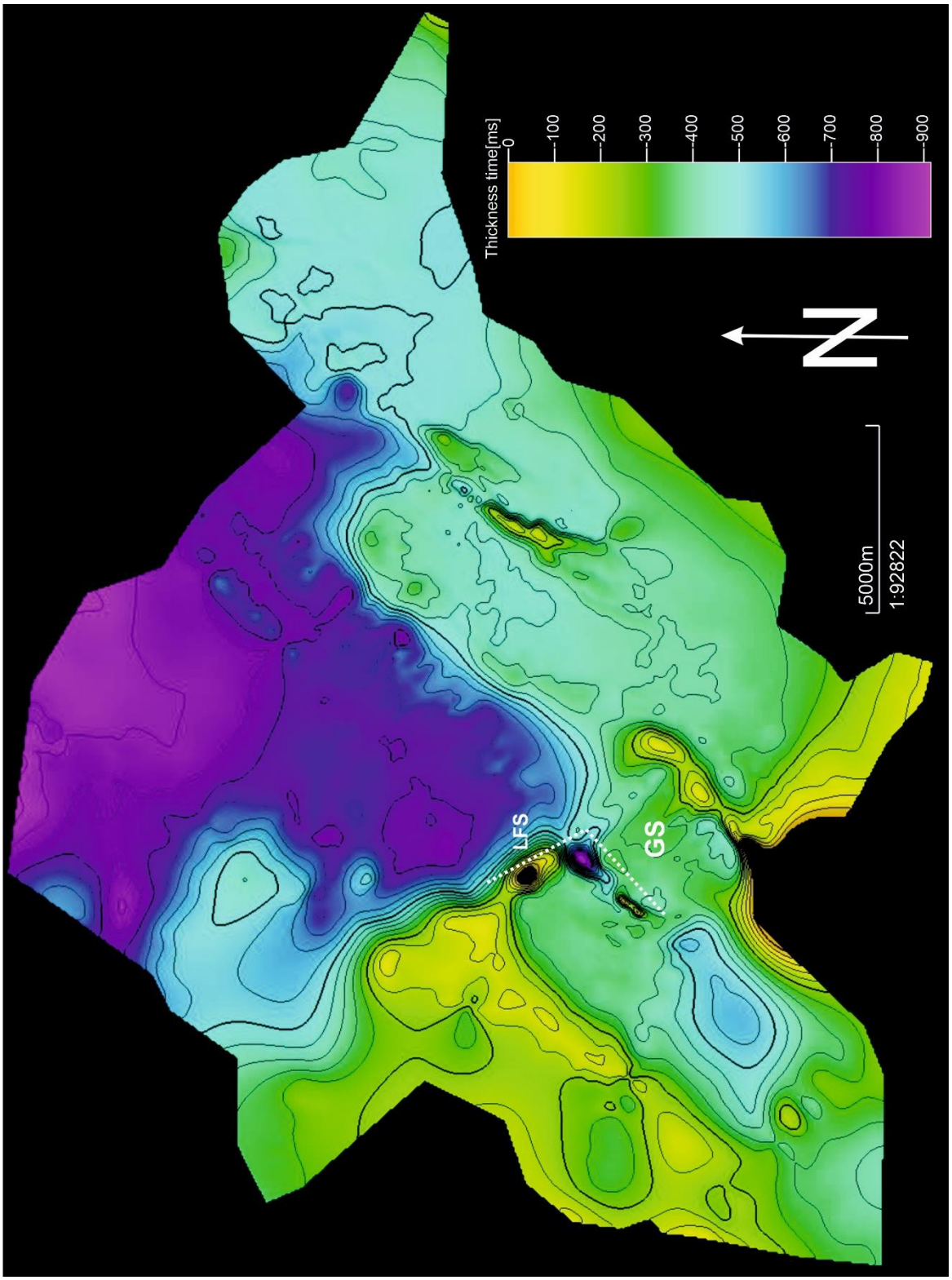

Figure 15: Thickness map of the Sarmatian package showing maximum thicknesses of around 900ms.

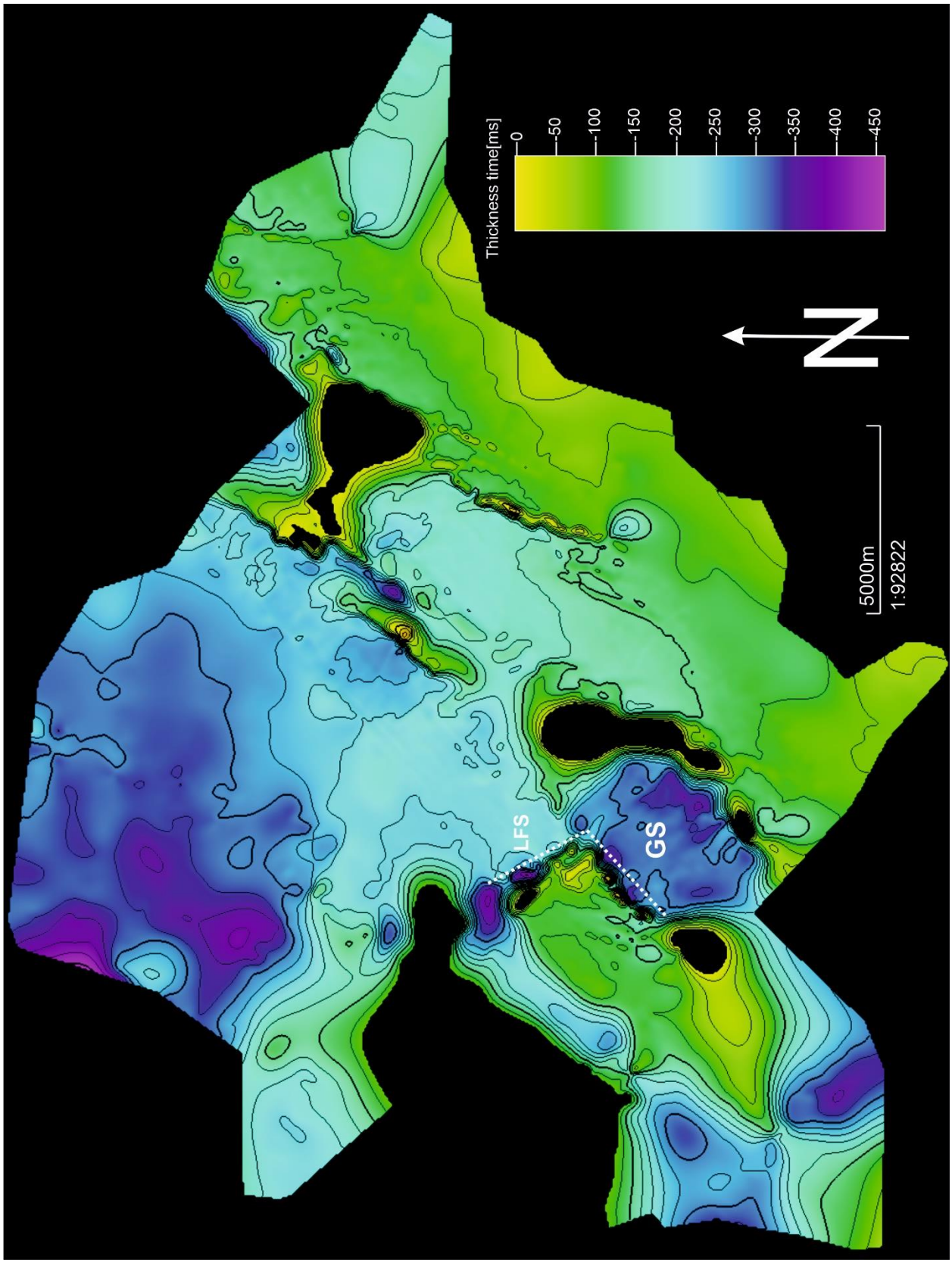

Figure 16: Thickness map of the Pannonian package. Maximum thicknesses reach c. 450 ms.

4.4 Structural Setting

In this study, 88 different faults were interpreted (Table 4) and categorized into four main groups based on their location, strike, dip and size (Fig. 17). The main fault groups include (i) the Leopoldsdorf system (LFS), (ii) Western fault group (WFG), (iii) Graben system (GS) and (iv) Eastern faults group (EFG) and are described in detail below.

Number	Fault Group	Name	Fault Type	Strike	Dip	Aberrations	Color (in Petrel)
1	**Leopoldsdorf Fault System**	LFS-1	Normal	NNW-SSE	NE		Orange
2		LFS-2	Normal	NNE-SSW	NE		Purple
3		LFS-3	Normal	NE-SW	SE	Changes to NNW-SSE	Teal
4		LFS-4	Normal	NE-SW	SE	Changes to NNW-SSE	Blue
5		LFS-5	Normal	NE-SW	SE		Yellow
6		LFS-6	Normal	N-S	W		Blue
7		LFS-7	Normal	N-S	W		Orange
8		LFS-8	Normal	NNW-SSE	SE		Pink
9		LFS-9	Normal	NNW-SSE	NE		Green
10		LFS-10	Normal	NE-SW	SE		Blue
11		LFS-11	Normal			Single line	Green
12		LFS-12	Normal			Single line	Blue
13		LFS-13	Normal	N-S	E		Purple
14		LFS-14	Normal			Single line	Purple

15		LFS-15	Normal			Single line	Grey
16		LFS-16	Normal			Single line	Yellow
17		LFS-17	Normal	NNE-SSW	SE		Red
18		LFS-18	Normal	NE-SW	SE		Yellow
19		LFS-19	Normal			single line	Green
20		LFS-20	Normal			single line	Purple
21		LFS-21	Normal			single line	Yellow
22		LFS-22	Normal			single line	Red
23		LFS-23	Normal			single line	Purple
24		LFS-24	Normal			single line	Teal
25		LFS-25	Normal			single line	Green
26		LFS-26	Normal			single line	Blue
27		LFS-27	Normal			single line	Yellow
28		LFS-28	Normal			single line	Green
29		LFS-29	Reverse			single line	Blue
30		LFS-30	Normal			single line	Purple
31		LFS-31	Normal			single line	Yellow
32		LFS-32	Normal			single line	Red
33		LFS-33	Normal			single line	Green
34	**Graben System**	GS-1	Normal	NE-SW	SE		Red
35		GS-2	Normal	NE-SW	SE		Blue
36		GS-3	Normal	NW-SE	SW		Green

37		GS-4	Normal + Strike -Slip	NE-SW	NW	neg. flower structure	Orange
38		GS-5	Normal + Strike -Slip	NE-SW	NW	neg. flower structure	Purple
39		GS-6	Normal + Strike -Slip	NE-SW	NW	neg. flower structure	Red
40		GS-7	Normal + Strike -Slip	NE-SW	NW	neg. flowers tructure	Blue
41		GS-8	Normal + Strike -Slip	NE-SW	NW	neg. flower structure	Pink
42		GS-9	Normal + Strike -Slip			neg. flower structure single line	Blue
43		GS-10	Normal + Strike -Slip			neg. flower structure single line	Teal
44		GS-11	Normal + Strike -Slip			neg. flower structure single line	Green
45		GS-12	Normal + Strike -Slip			neg. flower structure single line	Yellow
46		GS-13	Normal	NE-SW	NW		Green

47		GS-14	Normal	NE-SW	NW		Yellow
48		GS-15	Normal	NE-SW	NW		Teal
49		GS-16	Normal	NE-SW	NW		Green
50		GS-17	Normal	NE-SW	NW		Red
51		GS-18	Reverse			Single line	Purple
52		GS-19	Normal			Single line	Green
53		GS-20	Normal	NE-SW	SE		Teal
54		GS-21	Normal	NE-SW	NW		Red
55		GS-22	Normal	NE-SW	NW		Yellow
56		GS-23	Normal	NE-SW	W		Blue
57		GS-24	Normal			Single line	Red
58		GS-25	Reverse			Single line	Orange
59		GS-26	Reverse			Single line	Purple
60		GS-27	Reverse			Single line	Teal
61		GS-28	Reverse			Single line	Yellow
62		GS-29	Normal			Single line	Green
63		GS-30	Normal			Single line	Blue
64	**Eastern Fault Group**	EFG-1	Normal	NE-SW	NW		Green
65		EFG-2	Normal	NE-SW	NW		Yellow
66		EFG-3	Normal			Single line	Blue
67		EFG-4	Normal			Single line	Pink

68		EFG-5	Normal			Single line	Orange
69		EFG-6	Normal			Single line	Red
70		EFG-7	Normal	N-S	E		Red
71		EFG-8	Normal	N-S	W		Purple
72		EFG-9	Normal	N-S	W		Orange
73		EFG-10	Normal	N-S	W		Blue
74		EFG-11	Normal	N-S	E		Pink
75		EFG-12	Normal	NNW-SSE	WSW		Green
76		EFG-13	Normal	NNW-SSE	ENE		Orange
77		EFG-14	Normal	N-S	W		Teal
78		EFG-15	Normal	NW-SE	SW		Pink
79		EFG-16	Normal	NW-SE	NE		Purple
80	**Western Fault Group**	WFG-1	Normal + Strike -Slip	NW-SE	SW		Green
81		WFG-2	Normal + Strike -Slip	NW-SE	SW		Yellow
82		WFG-3	Normal + Strike -Slip	NW-SE	SW		Blue
83		WFG-4	Normal + Strike -Slip	NW-SE	NE		Purple

84		WFG -5	Normal + Strike -Slip	NW-SE	NE		Pink
85		WFG -6	Normal + Strike -Slip	NW-SE	NE		Orange
86		WFG -7	Normal			Single line	Grey
87		WFG -8	Normal + Strike -Slip			Single line	Green
88		WFG -9	Normal			Single line	Teal

Table 4: List of interpreted faults on 2D Lines and inside the 3D-Cube Moosbrunn (OMV).

4.4.1 Leopoldsdorf fault system - LFS

The Leopoldsdorf fault system is one of the two large-scale fault zones that have been identified in the studied area of the southern Vienna Basin. Together with the Graben system they represent the major structural elements in the area. The LFS can be traced on both the 2D and 3D seismic data. Figure 17 gives an overview of its spatial evolution, being composed of numerous very steep faults with variable dips to the SE, NE and E. The change in their dips is given due to the changing strike of these faults. The strike of faults that belong to the LFS group changes abruptly from roughly NE-SW to the N-S (Figure 17). This bend of nearly 90 degrees is observed in the 3D seismic cube. Based on the seismic data, it seems that the LFS faults splays off the large-scale NE-SW trending faults belonging to the GS group (Figure 18a) or alternatively that they might be offset by basin-bounding faults of the GS group (Figure 17). Further west, the LFS fault zone becomes wider, and the faults constitute basin-bounding faults for sedimentary depocenter(s) further west and northwest. This topic is discussed separately in section 4.5. Given the seismic resolution, faults can be interpreted down to depth of 3600 ms TWT in the most northern parts of the 2D lines and down to 2500 ms TWT within the 3D cube. The LFS is tracked for more than 20 km on available seismic data but extends beyond the given dataset further north.

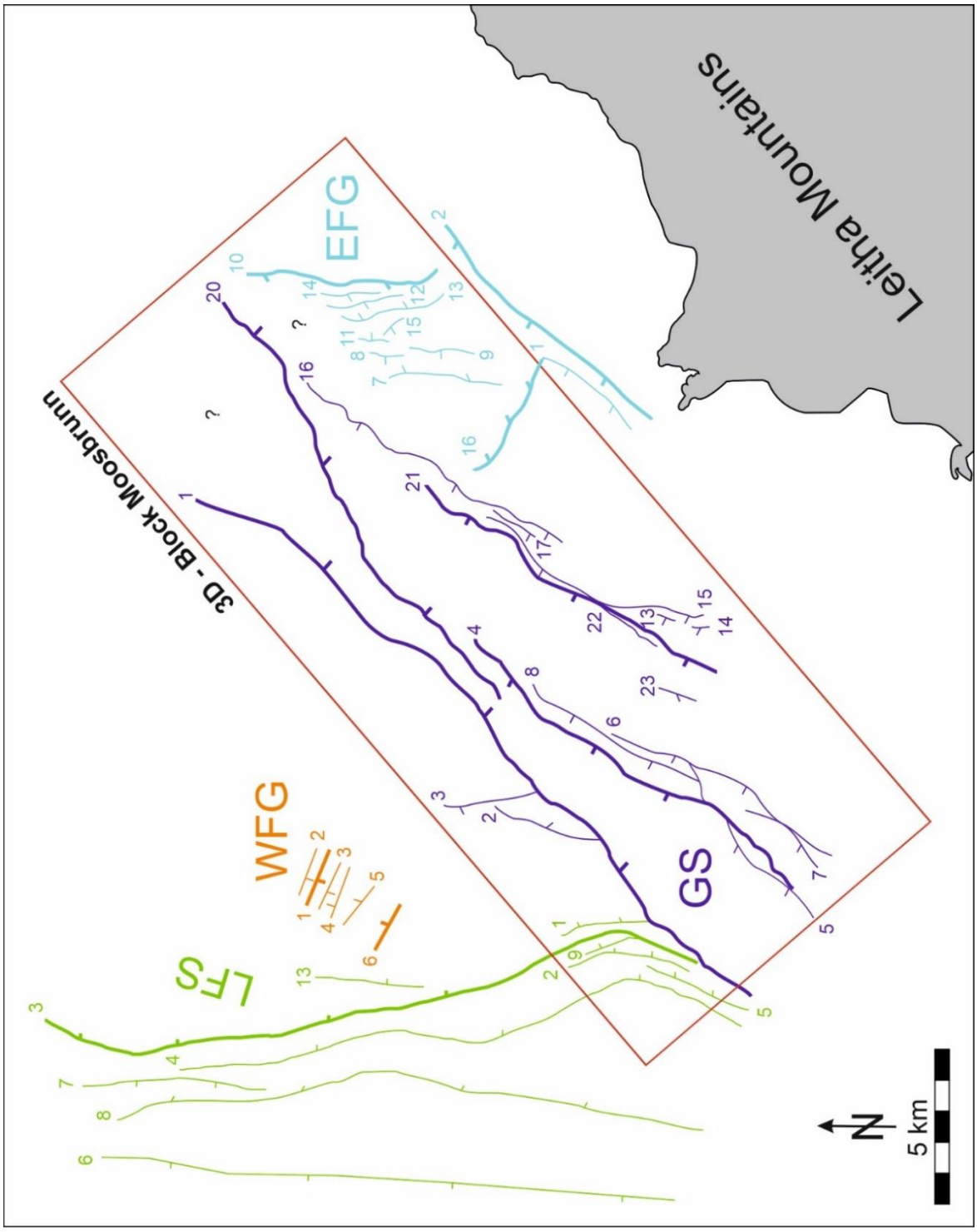

Figure 17: Structural map of the four main fault groups interpreted in the study (only important or large-scale faults are shown for each group). Abbreviation: LFS – Leopoldsdorf fault system, WFG – Western fault group, GS – Graben system, EFG – Eastern fault group.

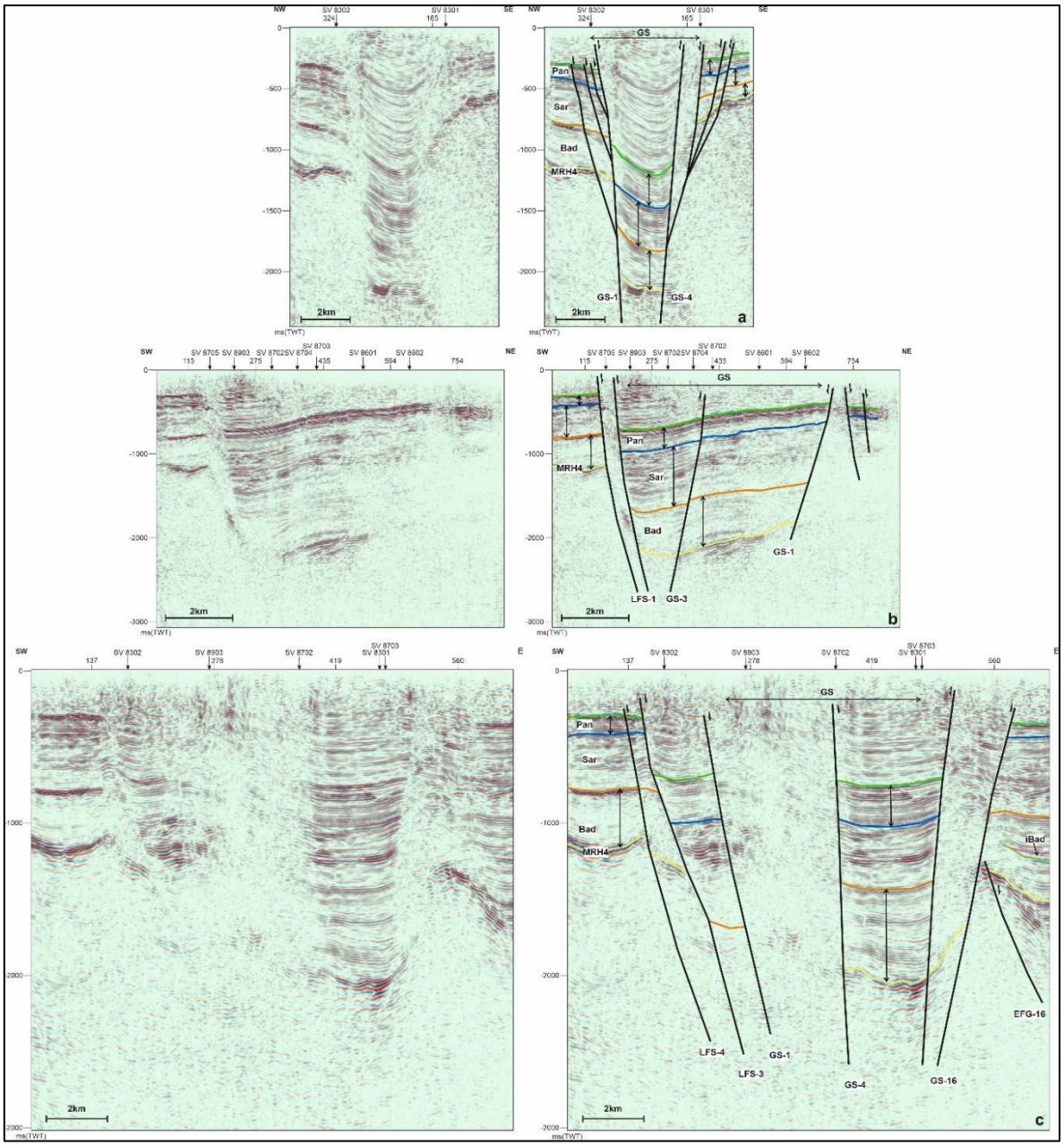

Figure 18: Spatial evolution of the Leopoldsdorf Fault System; a) seismic line XL100; b) seismic line IL367; c) seismic line CL1. Black double arrows indicate thickness changes within the individual seismic packages. Abbreviations: GS – Graben System. For location see Figure 12.

In the 3D seismic data, the Leopoldsdorf fault system is best displayed in the SW corner of the cube (Figures 19 and 20). Seismic packages Badenian, Sarmatian and Pannonian display significant thickness changes across fault LFS-1 (i.e., Figure 19). The majority of faults from the LFS group that are closely spaced with faults from the group GS (described below) have SE- to NE-dips and they appear to join one fault plane in the depth (Figure 20). In the southernmost part of the cube, the LFS -1 constitutes the western basin-bounding fault of the central graben GS, before it swings away towards the SW (Figure 20).

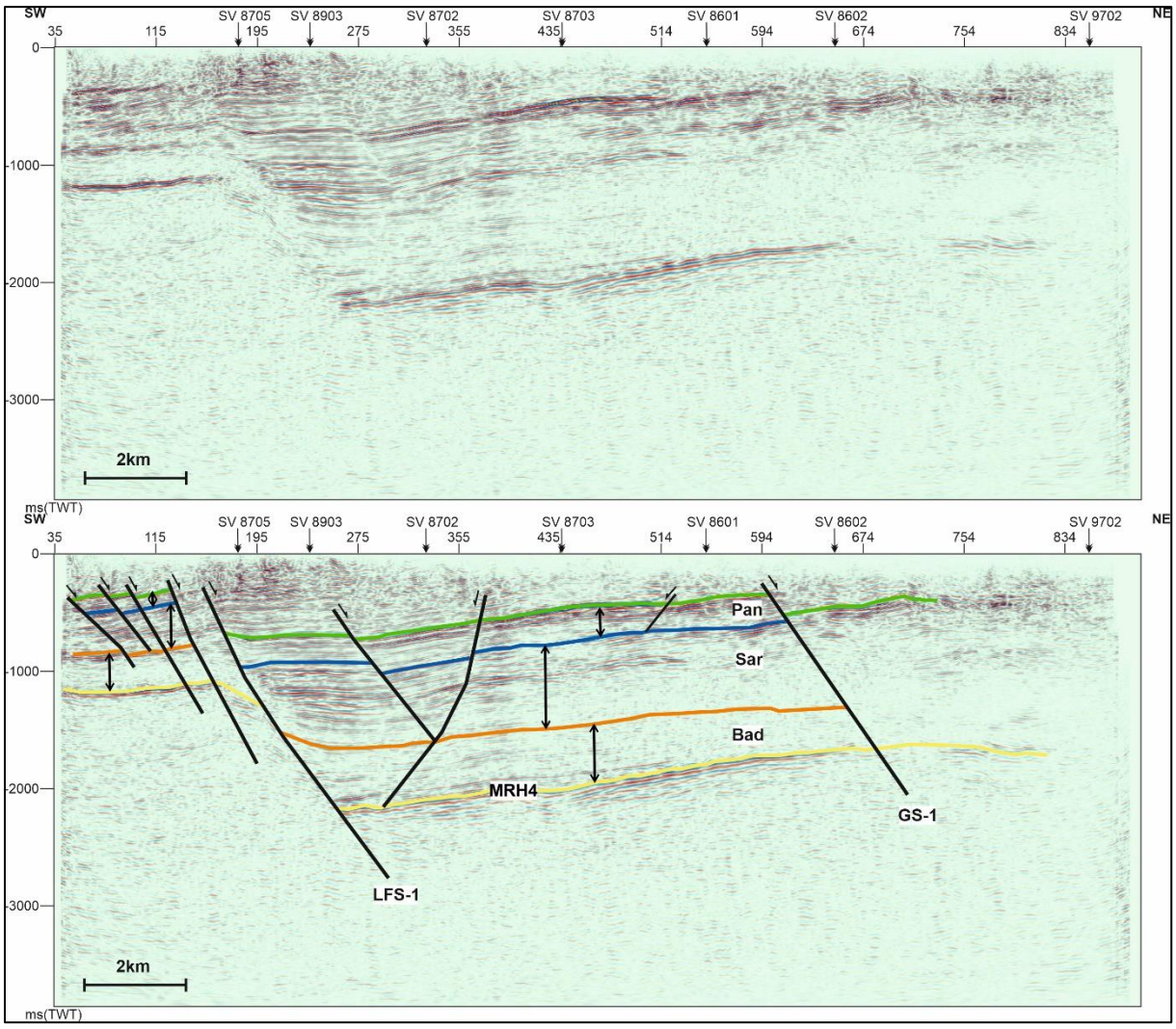

Figure 19: Seismic line IL 327 showing the four main packages as well as fault LFS-1, belonging to the Leopoldsdorf Fault System. Note poor seismic quality in the NE part of the cube that prevents interpretation of the seismic packages in that area. Significant stratal thickening within the packages across the fault LFS-1 is indicated by the black double arrows. The predominantly SE dipping normal faults can be interpreted down to c. 3000 ms TWT. For location see Figure 12.

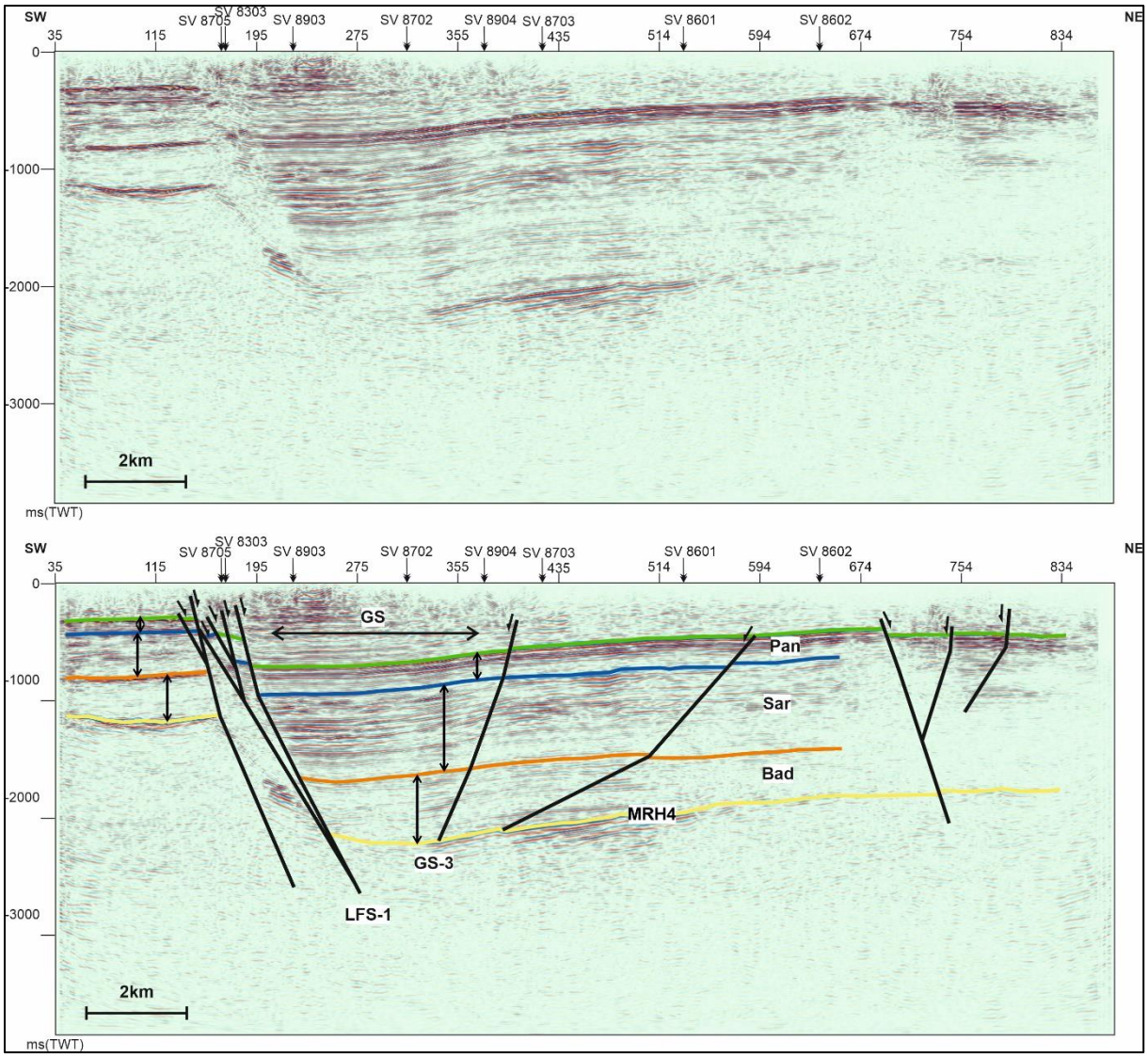

Figure 20: Seismic line IL 362 showing the Leopoldsdorf fault system (LFS) in the SW part of the seismic line with its most prominent fault, basin-bounding fault LFS-1. Stratal thickening is observed across fault LFS-1 for all packages (indicated by the black double arrows). The loss of seismic resolution does not permit any interpretation towards the NE part of the seismic cube. For location see Figure 12.

4.4.2. Western fault group – WFG

The interpreted faults which belong to the Western Fault group (WFG) are small faults (usually less than 3 km of lateral extent) that were interpreted on the 2D seismic lines only (Figures 17, 21 and 22). These faults have, however, greater lateral extent as documented in Salcher et al. (2012). The NW-SE striking faults are very steep, have SW and NE dips and can be traced to a maximum depth of c. 2000 ms TWT depending

on the seismic resolution (Figure 22). These faults are interpreted as antithetic adjustment faults related to the Leopoldsdorf fault system (represented by fault LFS-3 in Figure 22) and further discussed in section 4.5 dealing with 2D data in detail.

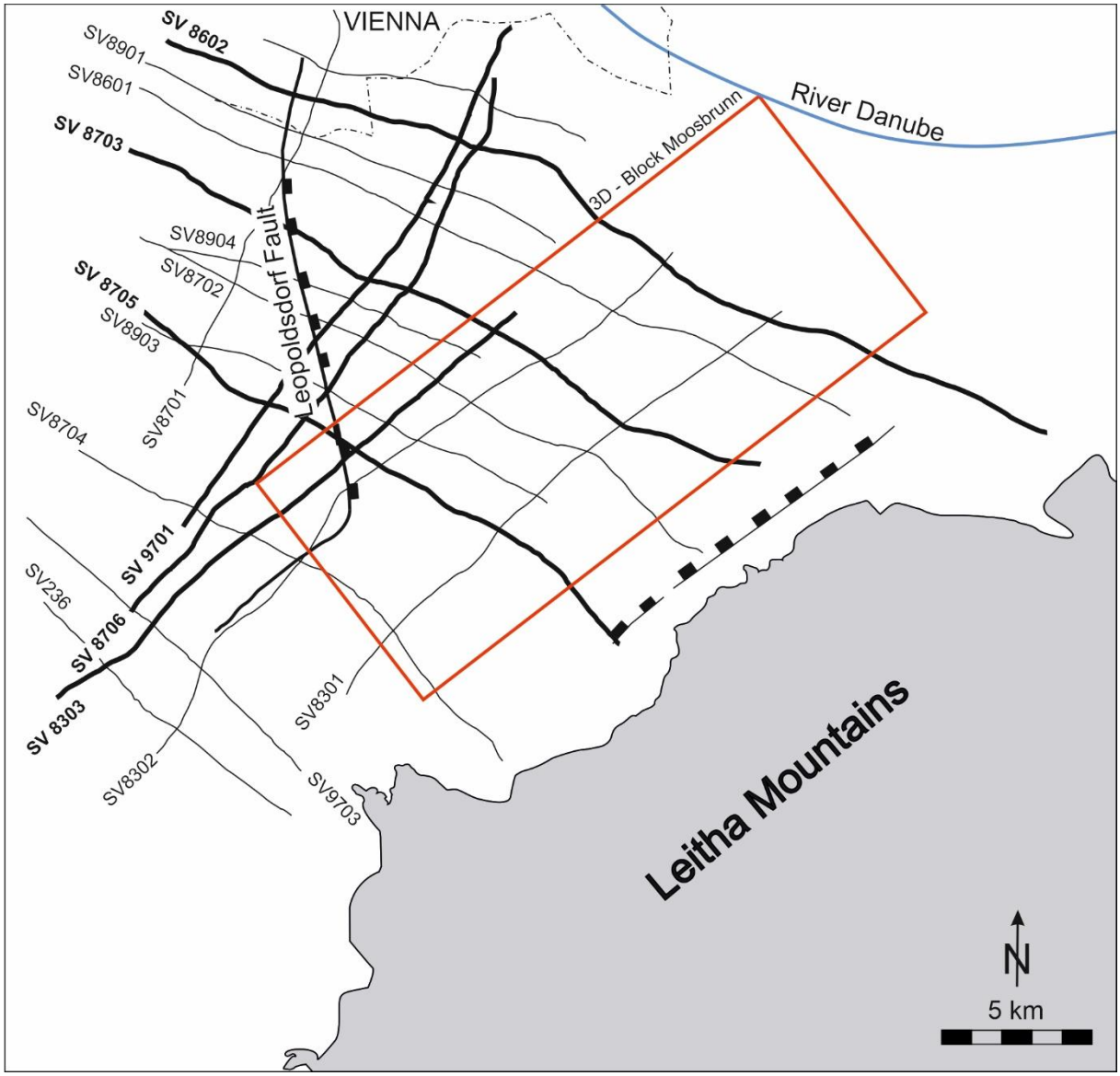

Figure 21: Location map showing 2D lines used in this study.

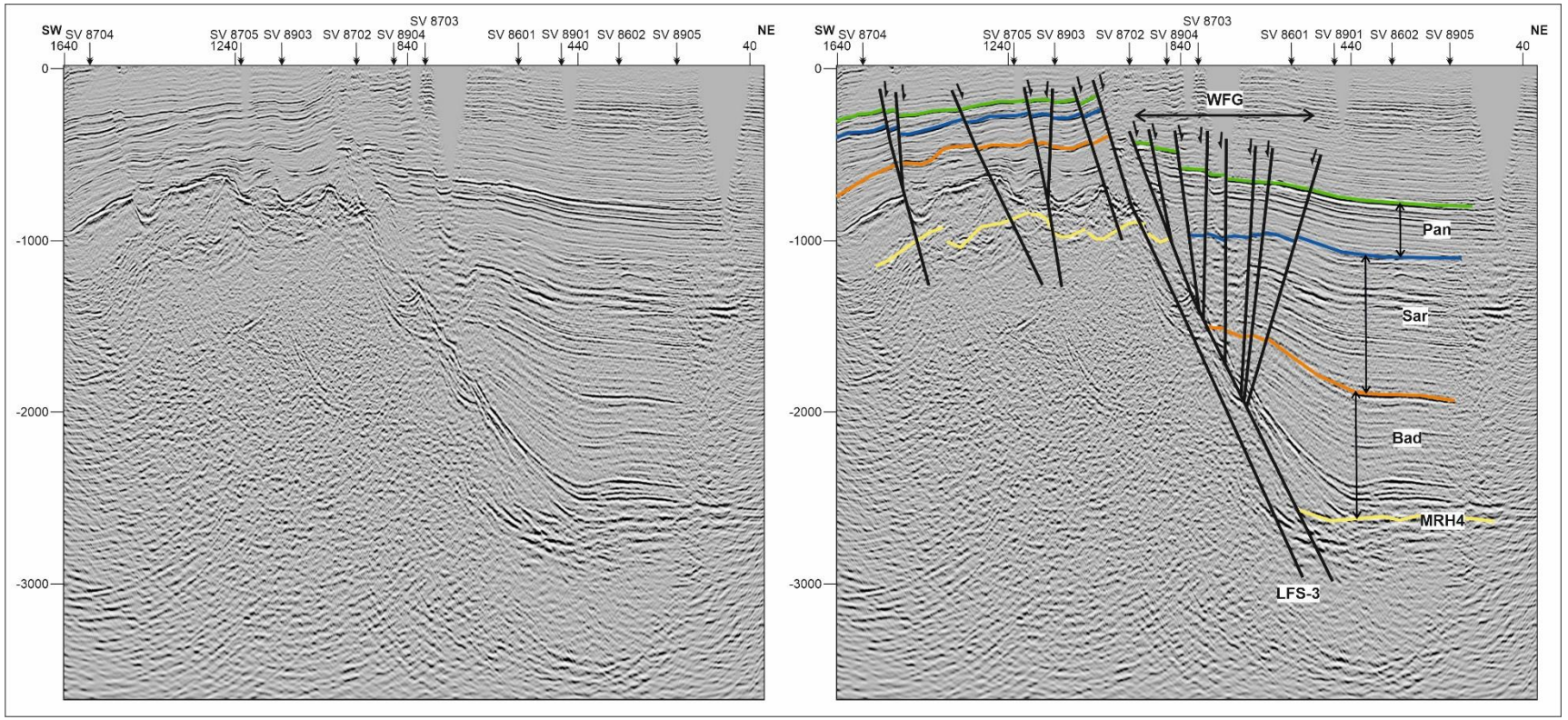

Figure 22: 2D seismic line SV9701 showing an example of the antithetic adjustment faults (WFG) related to the Leopoldsdorf fault system. Faults are very steeply dipping and offsetting all seismic packages, up to a minimal depth of around c. 2000 ms. VE: 2x. For location see Figure 21.

The Graben System (GS), the dominant structural element of the 3D cube, is a NE-SW trending large-scale fault system that is characterized by generally very steeply dipping normal faults. These can be interpreted down to c. 3000ms TWT; seismic resolution does not permit any further interpretation. Within the relatively narrow graben (shown as GS in Figure 23), seismic reflectors are diffuse, of low amplitude and cannot be traced laterally. The overall chaotic, low reflective character of the central graben is probably due to intense faulting and does not allow a detailed interpretation of seismic horizons (Figures 23 and 24). Additionally, the seismic reflectivity decreases north-eastwards as shown on NE-SW trending seismic line through the central graben (Figure 24).

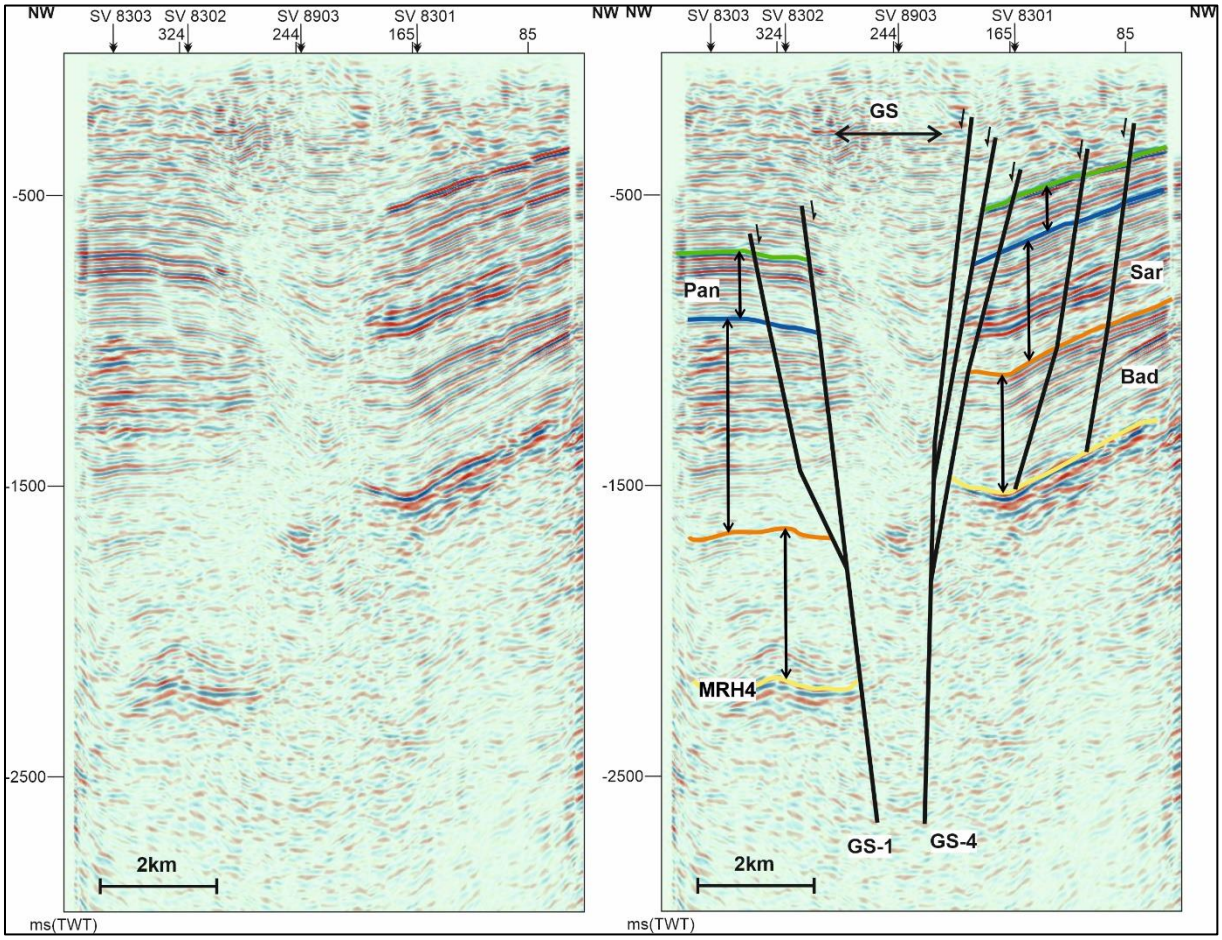

Figure 23: Seismic line XL 290 showing the poorly reflective narrow central graben (GS) bounded by two steep faults GS-1 and GS-4. The faults are tracked down to a depth of 2700ms TWT but are expected to extend much deeper. The faults form a negative flower structure. Stratal thickening is observed in all packages (indicated by the black arrows) and the most pronounce in the Badenian package. VE: 2x. For location see Figure 12.

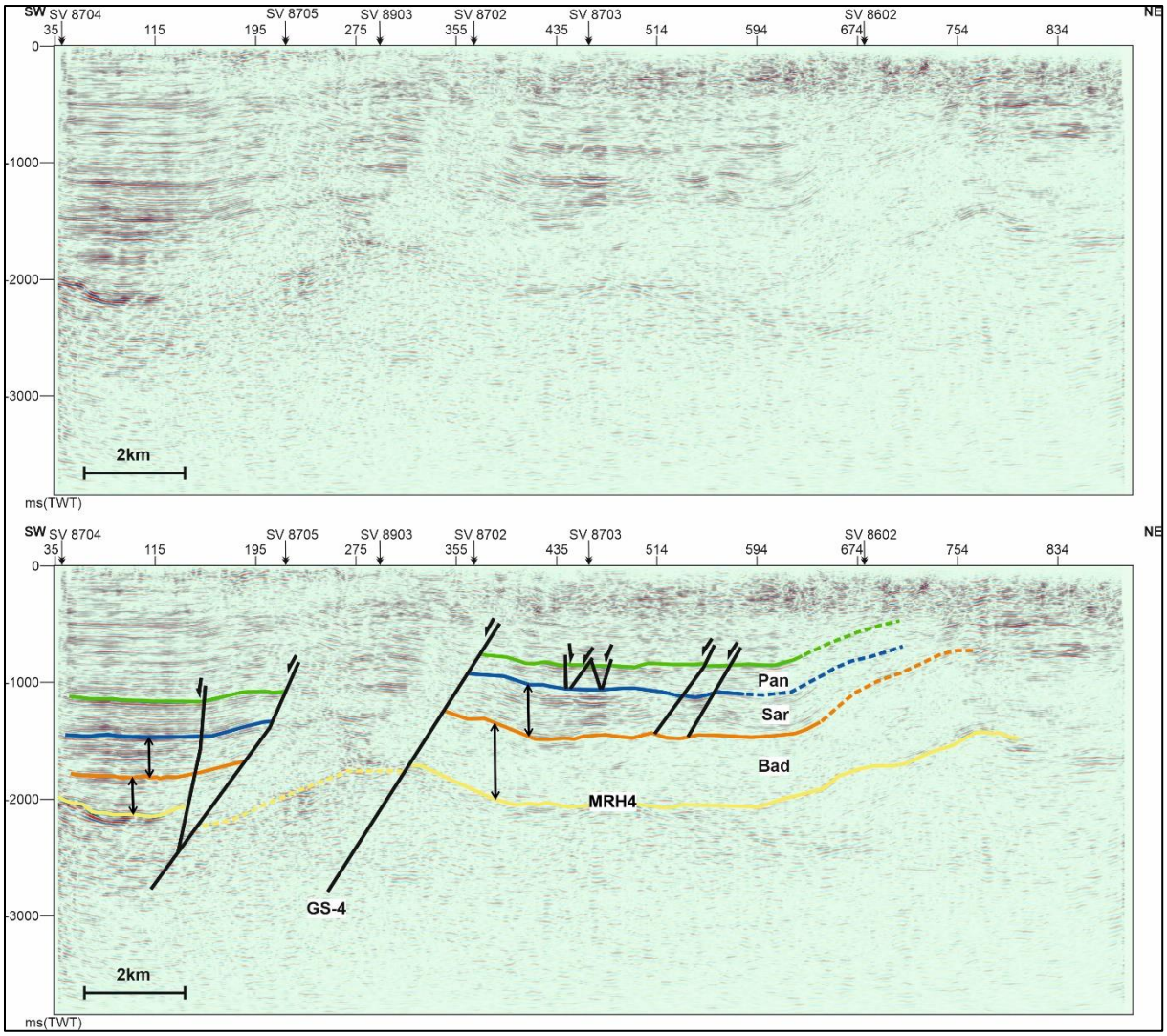

Figure 24: Seismic line IL 232 showing four main horizons and the poor seismic reflectivity along the strike of the central graben. The seismic resolution is very poor towards the NE (horizon interpretation is shown as dashed lines). Fault GS-4 represents a basin-bounding fault. Double black arrows indicate stratal thickening within the Badenian (Bad) and Sarmatian (Sar) packages. Abbreviations: GS-4 – Graben System fault-4, Bad – Badenian, Sar – Sarmatian. VE: 2x. For location see Figure 12.

However, in some parts of the GS, the seismic resolution allows to distinguish the seismic packages (Figures 25 – 27). Particularly, in the south, where the central graben is not to deep, the seismic reflectivity is reversed and it is better in the GS than along its flanks (Figure 26). The seismic line shown in Figure 26 is located at the edge of deep depocenter in the central graben (indicated as GS in Figure 16). Further north, the seismic reflectors in the GS also locally exhibit better lateral continuity (Figures 25 and 27).

Faults that constrain the central Graben system (GS) have opposite dips and often branch upwards to form a negative flower structure (Figures 23, 25 and 26). Along the western margin, two large-scale faults GS-1 and GS-20 dip to the SE and represent the basin-bounding faults (Figure 17). The eastern margin of the graben is defined by three large right-stepping normal faults with NW-dip, namely GS-4, GS-21 and GS-16 (Figure 17).

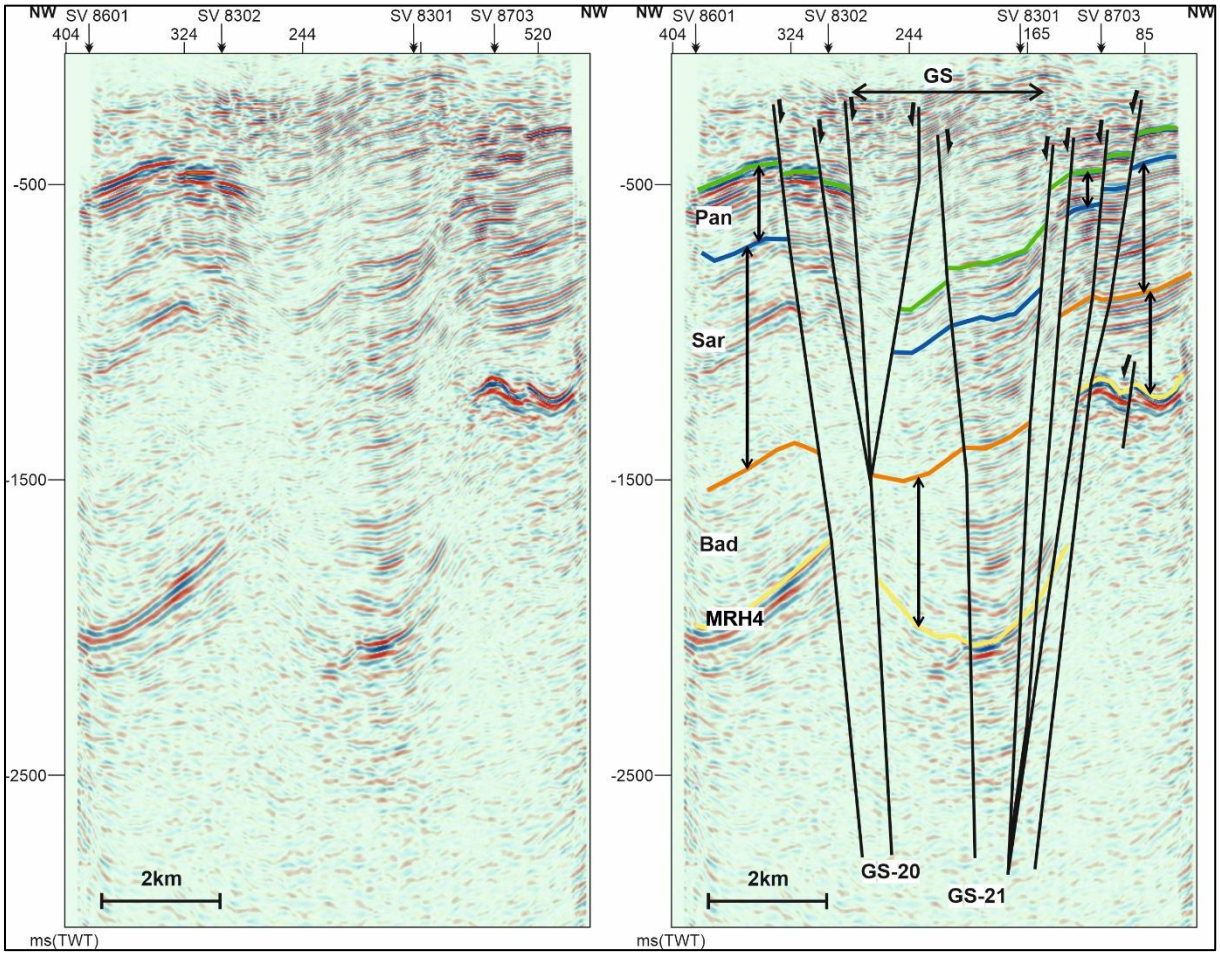

Figure 25: Seismic line XL 520 showing structural configuration of the northern segment of the central graben (GS), defined by opposite-dipping faults GS-20 and GS-21. Stratal thickening within the seismic packages is shown by the double black arrows. The seismic reflectivity is locally better and reflector are laterally continuous within the central part of the graben. VE: 2x. For location see Figure 12.The southern segment of the central graben GS is illustrated in Figures 23 and 26. The segment is located more to the west, when compared to the northern segment, and it is defined between faults GS-1 and GS-4. The polarity of the graben is towards the south-east. In contrast, the northern segment of the graben system exhibits north-western polarity, is laterally offset from the southern counterpart (Figure 17) and is defined by faults GS-20 and GS-21 (Figure 25).

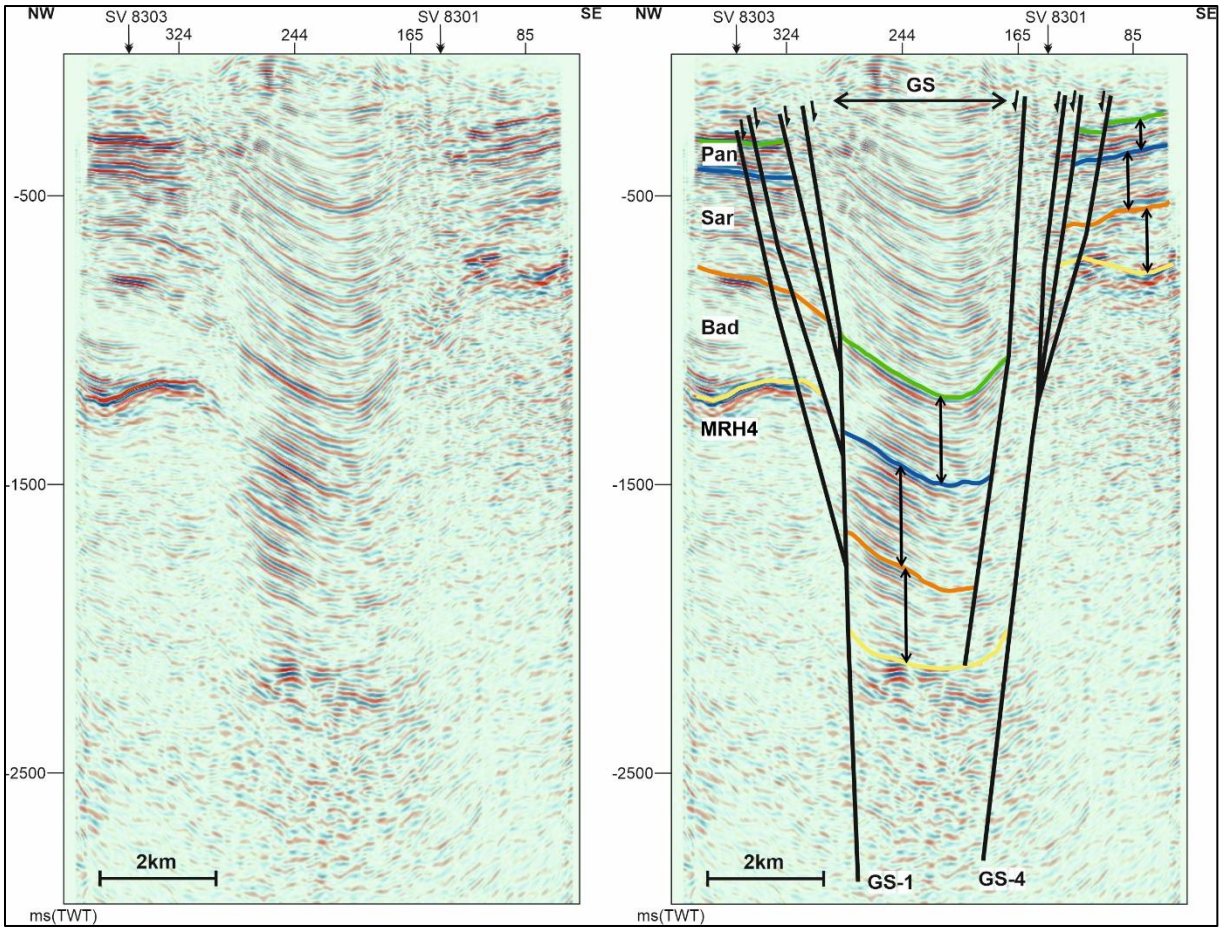

Figure 26: Seismic line XL 120 showing an example of the southern segment of GS and negative flower structure. Note the south-eastern polarity of the narrow graben. VE: 2x. For abbreviations see Figure 11. For location see Figure 12.

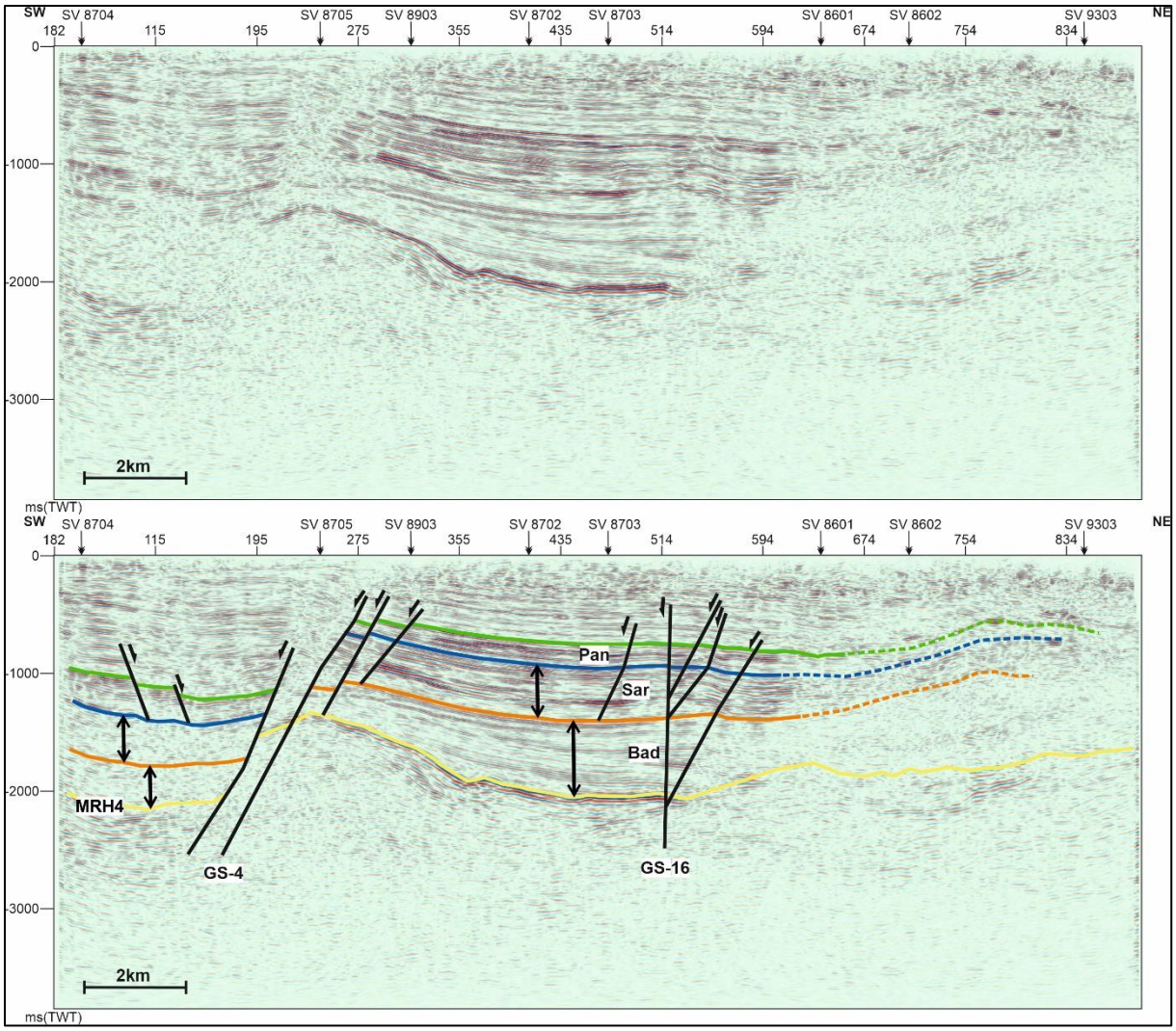

Figure 27: Seismic line IL 182 showing along-strike section and thickening of Badenian and Sarmatian packages towards fault GS-16 (illustrated by black double arrows). The steep, almost vertical normal faults GS-16 is interpreted as oblique-slip fault. The seismic line also shows the southern and northern segments of the central graben GS. Southern segment is delimited by fault GS-4, while the northern segment by fault GS-16. For location see Figure 12.

4.4.4. EFG – Eastern fault group

The Eastern fault group (EFG) was interpreted predominantly in the 3D seismic block (Figure 17), with only two NE-SW trending faults interpreted on the 2D lines just east of the 3D cube (faults EFG-1 and EFG-2 in Figure 17). In the 3D cube, the faults are concentrated in the NE part and have predominant N-S strike with E- or W-dip. Fault EFG-16 with its NW-SE strike is an exception (Figure 17). The EFG faults are rather small-scale when compared to the faults from the groups LFS and GS. Most of them do not offset the top of the basement package but terminate in Badenian and Sarmatian packages (Figures 28 and 29) or rarely in the Karpatian package (Figures 28 and 30, e.g., fault EFG-7).

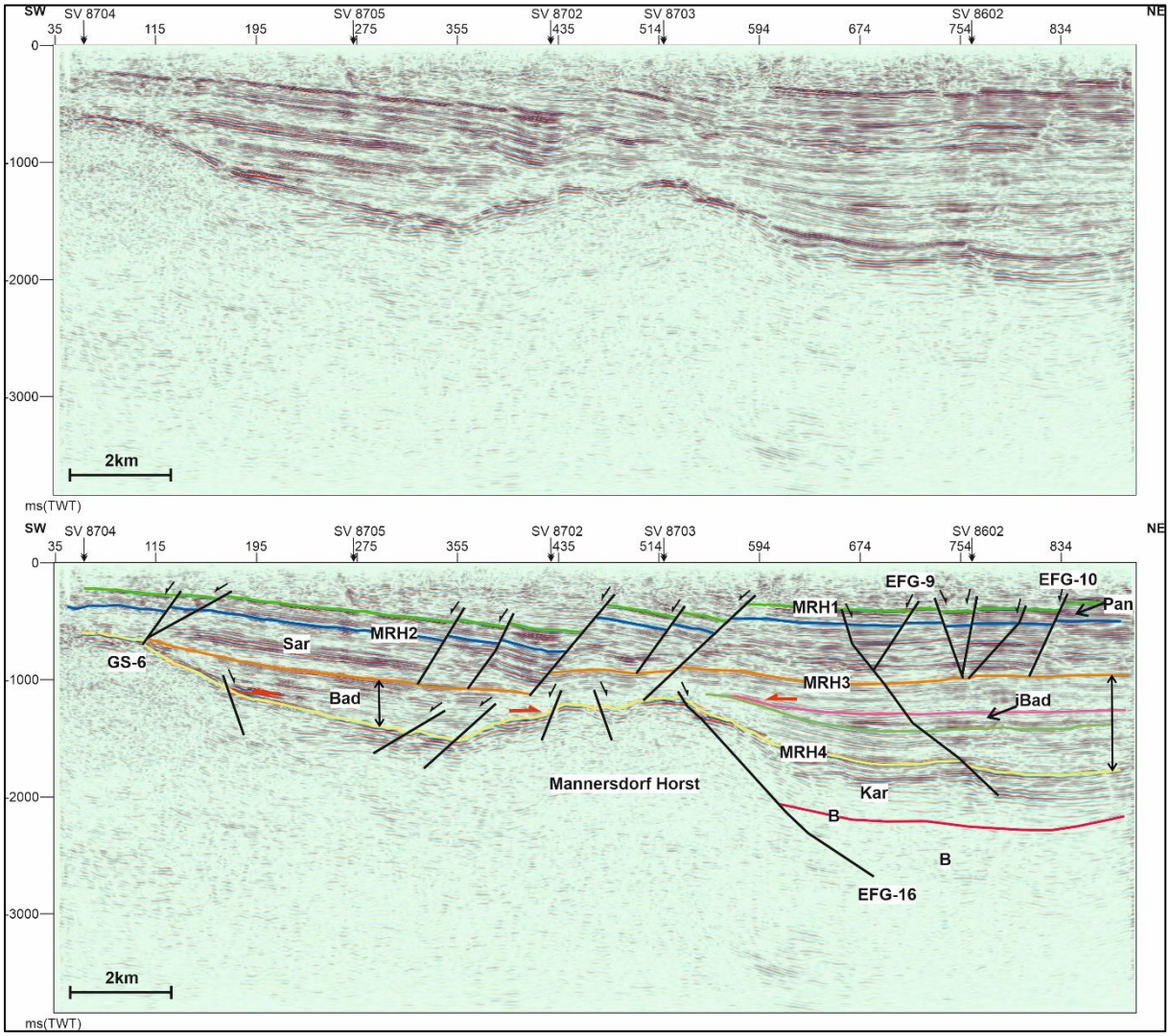

Figure 28: Seismic line IL 117 showing an example of the EFG in the NE part of the 3D cube. Fault EFG-16 is interpreted to controlled the depositional limit of the basement package (B). Smaller normal EFG faults commonly terminate in the Sarmatian (Sar) and Badenian (Bad) packages. For location see Figure 12.

The dips of the faults are shallower when compared to the other fault groups, especially to the faults belonging to the adjacent central graben (GS). Fault EFG-16 exhibit particularly shallow dip and it seems to be offset by fault GS-16 (Figure 30). The relationship, i.e., the termination of the faults, cannot be determined due to the poor quality of the seismic data in that area (shown by question mark in Figure 17).

Small onlaps can be identified within the Badenian seismic package, especially in the succession just above the intra-Badenian package (shown as iBad in Figures 28 and 29), but also along the central ridge (the Mannersdorf Horst), which is controlled by fault EFG-16 along its northern flank (Figures 28 and 29).

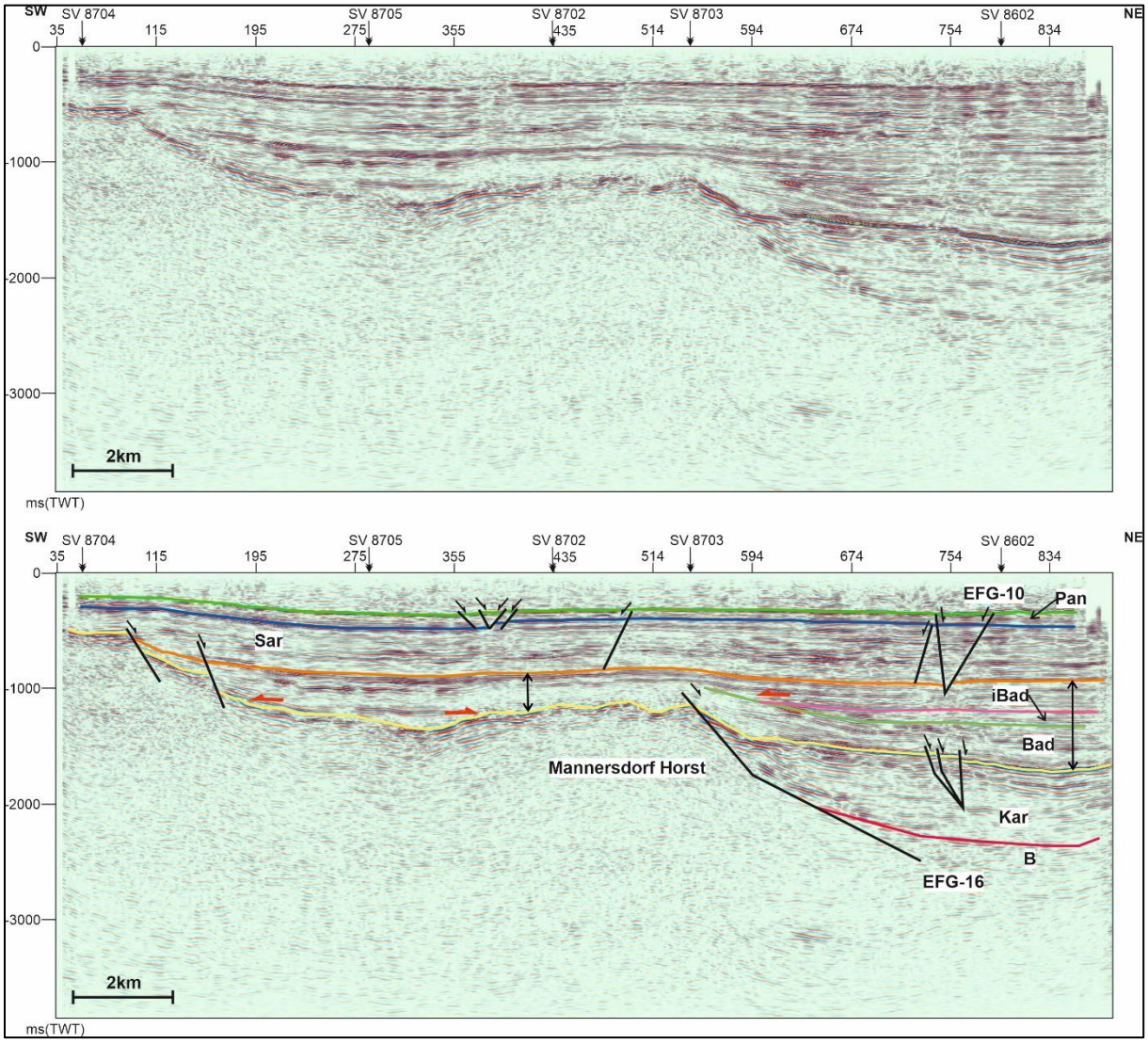

Figure 23: Seismic line IL67 showing thickness changes across the central ridge within the Badenian package as indicated by black double arrows. One of the largest EFG fault, fault EFG-16, seems to control regional extent of the Karpatian package. Onlaps in the Badenian package are shown by red arrows. For abbreviations see Figure 11. For location see Figure 12.

Significant thickness changes across the central ridge are observed in the Badenian package. Thickness of the strata increases towards the NE and the sudden increase in thickness spatially coincide with the location of fault EFG-16. The fault reaches, unlike the other, a depth of almost 3000 ms (TWT).

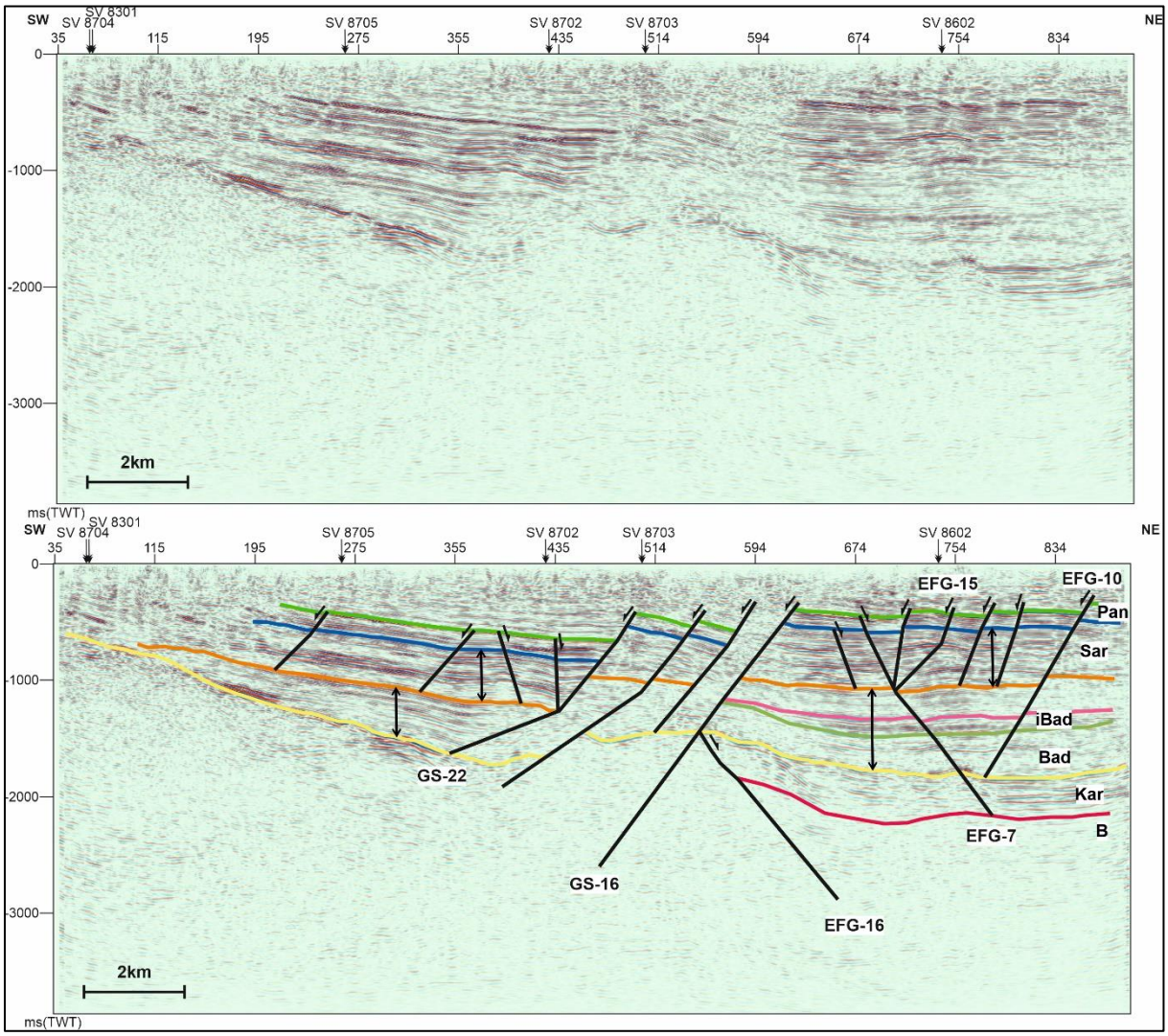

Figure 30: Seismic line IL 137 showing the main seismic packages in the NE part of the cube. Significant stratal thickening is observed within the Badenian package across the central ridge (shown by the black double arrows). Faults terminate in Sarmatian and Badenian packages, with exceptions of faults EFG-7 and EFG-16. For abbreviations see Figure 11. For location see Fig. 12.

4.5 2D Lines

The quality of the data of the 2D data set is good with generally medium to high amplitude laterally continuous seismic reflectors. The seismic resolution gradually deteriorates with depth, so that any consistent interpretation cannot be usually performed bellow 2500 - 3000 ms TWT (e.g., Figure 31). However, in some cases, the large-scale faults can be followed down to depths of c. 3600 ms TWT (Figure 32). The four main seismic packages shown in Table 3 can be distinguished on the 2D seismic lines. The local intra-Badenian seismic horizons that define the intra-Badenian seismic packages (Table 2 and Figure 7) are not interpreted along the 2D lines as only two 2D lines cross the NE corner of the 3D seismic cube and due to poor quality of the seismic data it has not been possible to pick them with certainty. Stratal thickening, indicated by white arrows in all figures below, can be observed throughout all the seismic packages. Most obvious growth strata in the Badenian, Sarmatian and also, to a lesser extent, in the Pannonian packages are observed along the faults belonging to the Leopoldsdorf fault system (LFS).

Next to the Leopoldsdorf Fault system (LFS), the large-scale NE-SW trending Graben System fault zone (GS) represents a major structural element and can be interpreted with certainty on 2D lines and linked to the 3D data (Figures 33 and 34). In contrast to the 3D seismic data, the continuity of seismic reflectors, and in general the seismic reflectivity is much better on 2D lines. Seismic reflectors within the GS are either relatively continuous across the fault zone (Figure 31) or they lack continuity and have low amplitude, so they cannot be interpreted with such certainty and are shown with dashed lines (33).

The biggest depocenter which is shown in the northwest segments of the time thickness maps in Figures 14-16 is situated north of the Leopoldsdorf Fault (represented by fault LFS-3 in Figure 35). The seismic packages Badenian and Sarmatian exhibit pronounced thickness changes across this fault. Roughly E-W trending seismic line shown in Figure 32 shows syn-sedimentary faulting during the deposition of Badenian and Sarmatian packages along the fault LFS-3. It is also assumed that faults from the group GS (represented by fault GS-20 in Figure 32) exhibit syn-sedimentary faulting during deposition of those packages.

Figure 35 additionally depicts small-scale faults of the group WFG. Some of them form antithetic adjustment faults to main fault LFS-3. The detailed mapping of these faults is not possible as they only occur on the 2D lines. However, due to their restricted regional extent, they do not represent major structural elements in the studied area.

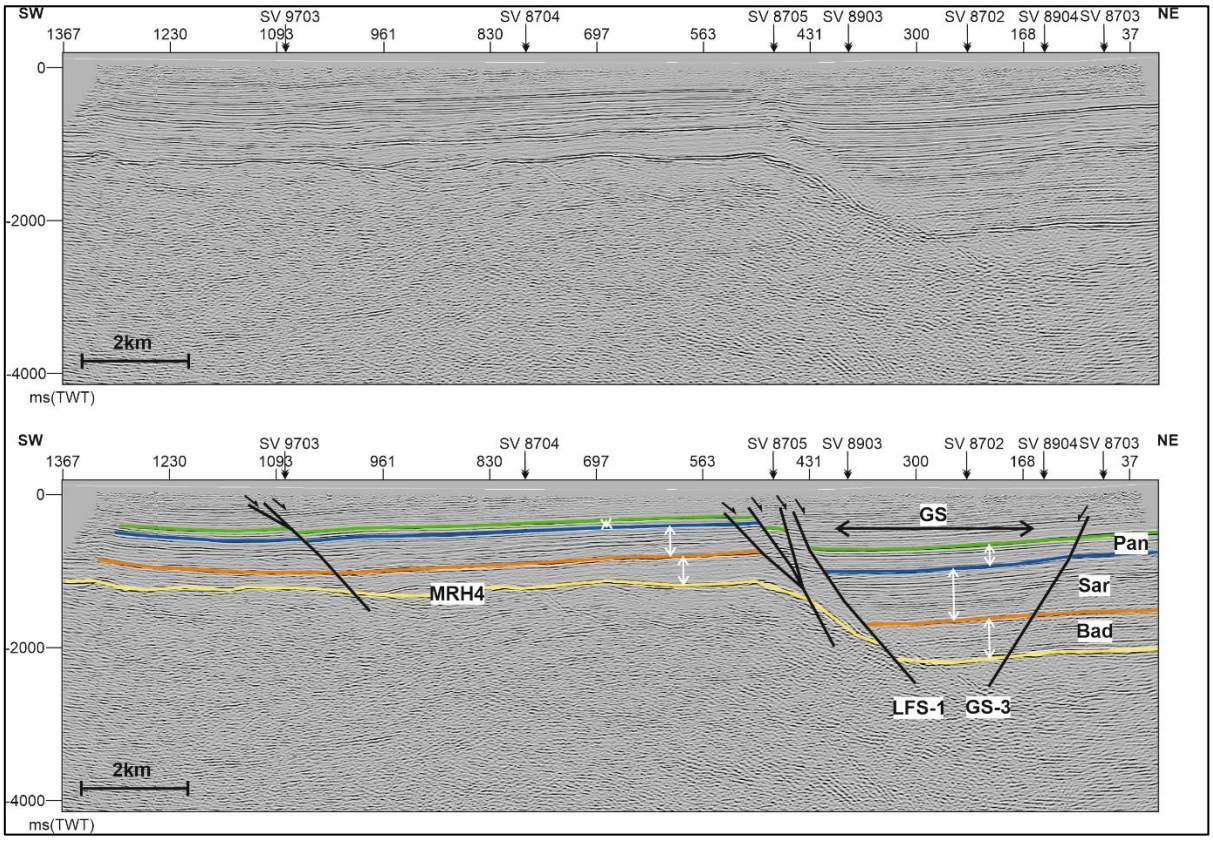

Figure 31: 2D seismic line SV8303 showing the four main seismic packages. Stratal thickening occurs across faults LFS-1 towards the NE within Badenian to Pannonian packages (indicated by white arrows). N-S trending faults LFS-1 and GS-3 constitute the western and the eastern margin of the depocenter (GS) respectively. The depocenter is located outside the main central graben, but it is jointly controlled by faults from both groups LFS and GS. Abbreviations: LFS-1 – Leopoldsdorf Fault System-1, GS-3 – Graben System Fault. For location see Figure 21.

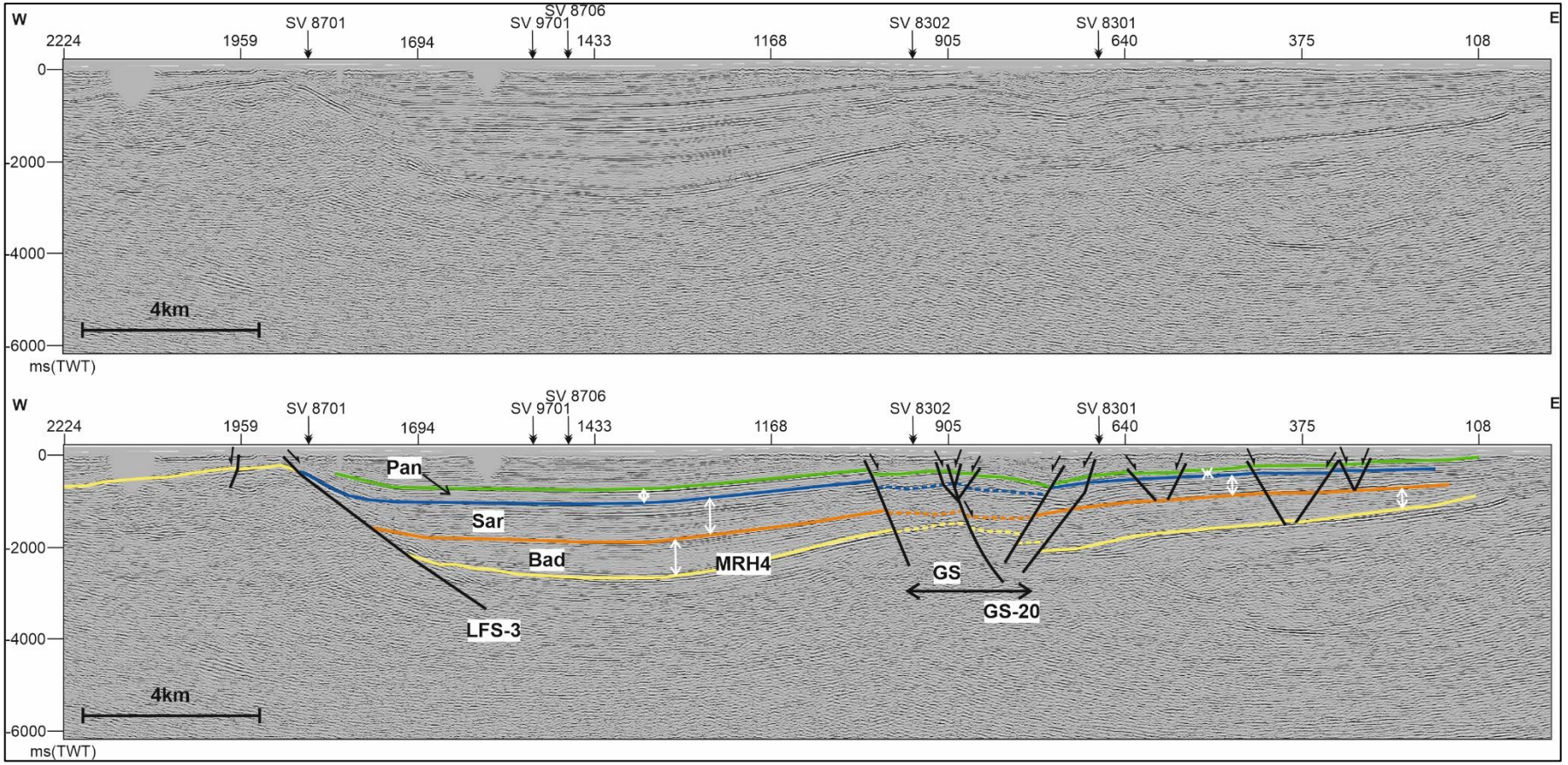

Figure 32: 2D seismic line SV8602 showing the four main seismic packages with increasing thickness towards fault LFS-3 in the west of the studied area (shown by white arrows). Seismic reflectios in the central graben (GS) are weaker and therefore the interpreted packages are shown in dashed lines. Fault LFS-3 can be interpreted to a minimum depth of c. 3500 ms TWT. Fault GS-20 is a prominent feature within the Graben system (GS) and is also interpreted to be syn-sedimentary at least during the deposition of the Badenian package. Abbreviations are found in Figure 11. For location see Figure 21.

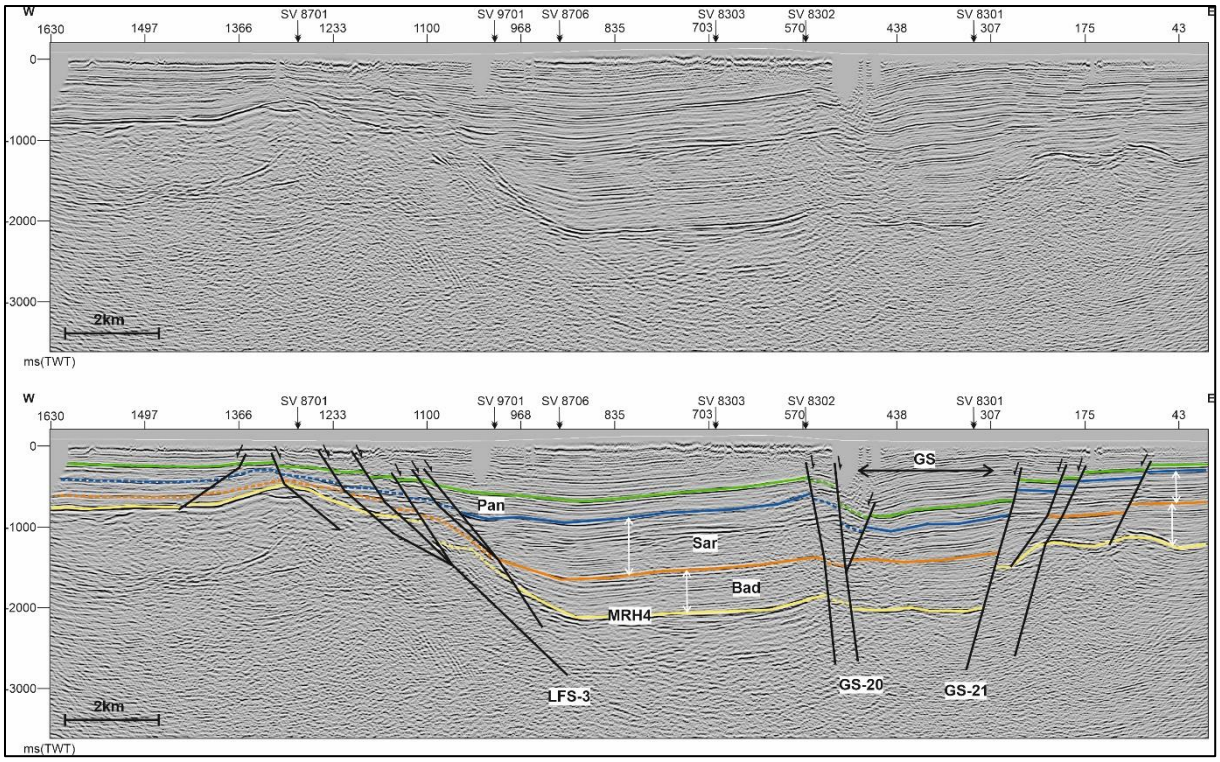

Figure 33: 2D seismic line SV8703 showing the Leopoldsdorf fault group (exemplified by fault LFS-3 and adjacent faults). Stratal thickening of the Sarmatian and Badenian package is indicated by the white double arrows. Faults of the LFS group have shallower dips when compared to the faults that belong to the central graben (GS-20 and GS-21) in the eastern part of the line. For abbreviations see Figure 11. For location see Figure 21.

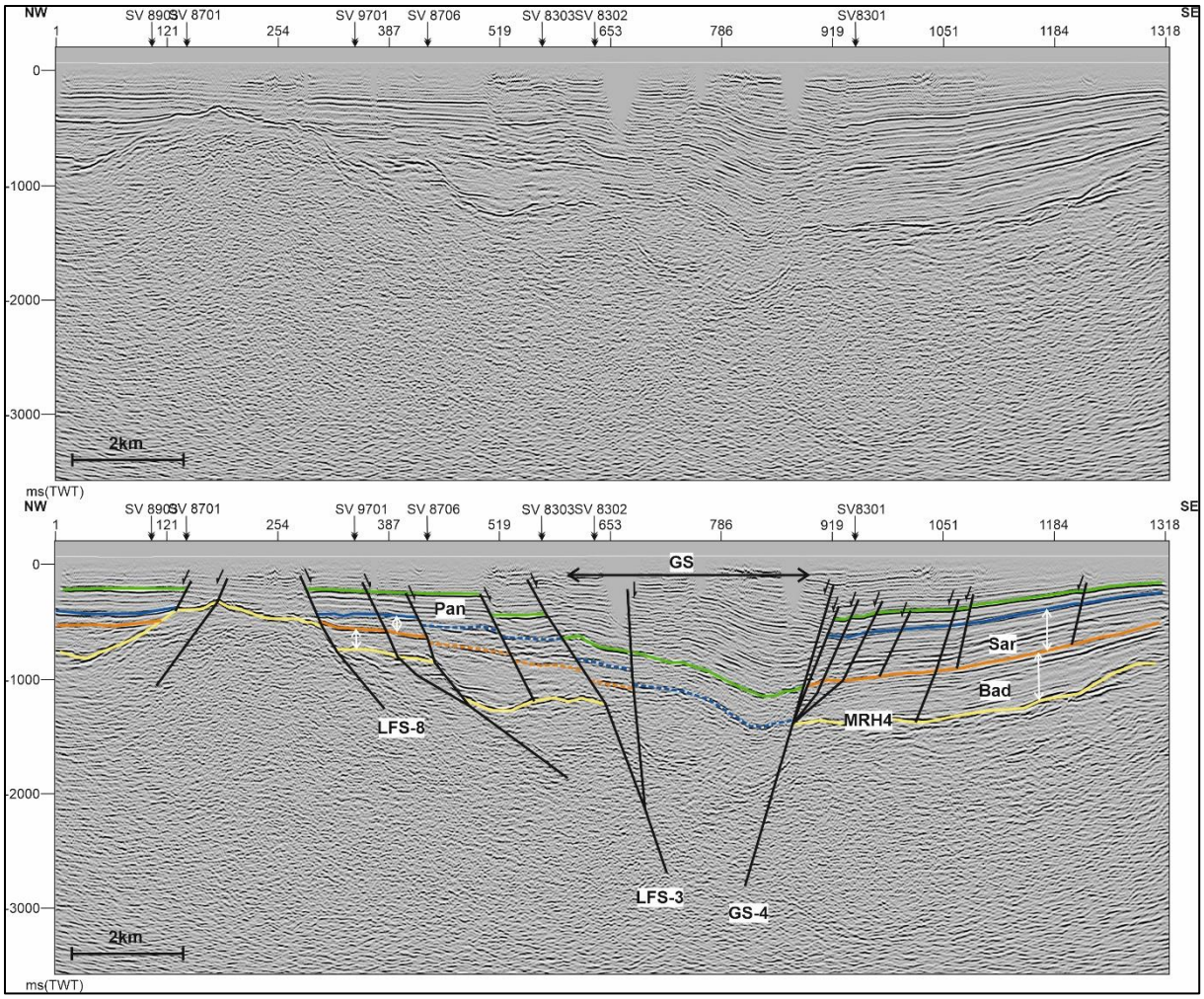

Figure 34: 2D seismic line SV8705 showing the structural configuration of the southern part of the studied area with its four main seismic packages. They can be easily distinguished along the line except for the central Graben System (GS) where the seismic resolution is poor. Increase in thickness towards the east is observed within the Sarmatian (Sar) and Badenian (Bad) packages (illustrated by the white arrows) but cannot be linked clearly to one of the interpreted faults. Steep faults GS-4 with a NE-SW strike and NW dip represents an eastern basin-bounding fault of the central graben (GS). The LFS group is exemplified here by a suite of faults with similar dips, e.g., fault LFS-3 and LFS-8. Fault LFS-3 constitutes the western margin of the central graben, further north it swings away to the west. Abbreviations: GS – Graben System, for location see Figure 21.

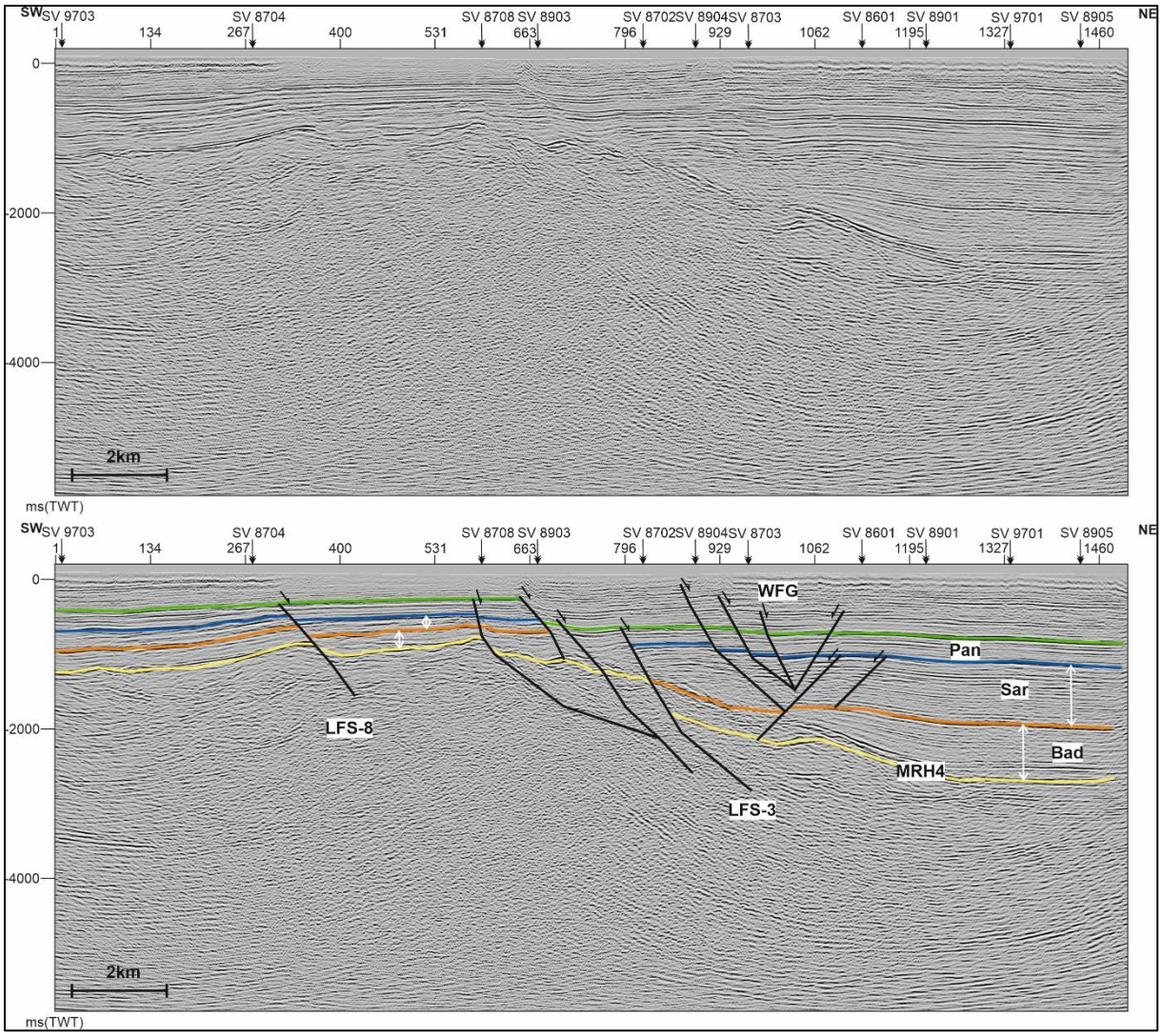

Figure 35: 2D seismic line SV8706 showing the four main seismic packages outside the 3D cube, only constrained on the 2D lines. Increase in thickness of the Sarmatian (Sar) and Badenian (Bad) packages can be observed generally towards north and is indicated by the white double arrows. The maximum thickness in the north (the largest depocenter in the studied area) is also shown in time thickness maps in Figures 14-16. The figure illustrates a structural configuration and relationship of the groups LFS (e.g., faults LFS-8 and LFS-3) and only locally occurring WFG. Abbreviations shown in Figure 11. For location see Figure 21.

Chapter 5: Discussion

Many previous studies on the Miocene succession in the Vienna Basin focused on analysis of individual structures at the field scale or based on seismic data, either in the northern and central parts of the Vienna Basin or in its southernmost part, the Mitterndorf Basin (e.g., Hölzel et al. 2010, Beidinger and Decker 2011, Salcher et al. 2012, Decker 1996). This study focused on the area, which is covered by Moosbrunn 3D seismic block and older 2D lines, and which has been described in relatively few publications in detail (e.g., Hinsch et al. 2005, Strauss et al. 2006). The studied region spans the northernmost segment of the Mitterndorf Basin and, in a more general term, the southern part of the Vienna Basin. The main focus was to interpret faults that offset the Miocene sedimentary basin fill and to document thickness changes of individual seismic packages that might be related to a Miocene syn-sedimentary activity of those faults. This chapter includes discussion on (i) thickness changes of individual seismic Miocene packages, (ii) lateral shift of depocenters throughout Miocene times and (iii) structural setting of the studied area.

5.1 Thickness changes

The thickness changes are observed in all interpreted packages except for the oldest Karpatian package. In this case, Karpatian strata are only interpreted in the NE part of the 3D seismic cube with certainty and their extent is most probably controlled by normal fault EFG-16, which constitutes the northern flank of the Mannersdorf Horst (Figure 28). However, as illustrated in Figure 30, the Karpatian packages exhibits subtle thinning towards fault EFG-16. On the other hand, it is difficult to interpret the Karpatian package in the remaining area of the 3D cube and also along the 2D lines due to generally low seismic resolution below the regional horizon MRH4. In the central system (GS), horizon MRH4 is particularly difficult to interpret and is only estimated at a minimum depth of c. 2500 ms (TWT) in places with low resolution and no well control. It must be hence assumed, that the horizon could lie much deeper.

The younger seismic packages Badenian, Sarmatin and Pannonian all exhibit significant thickness changes across a number of faults. The packages are well defined throughout the whole studied region, except for the NE part where the thicknesses are

not that well constrained due to poor-quality of the data. The most significant stratal thickening is interpreted to occur in the Badenian package. The thickness changes are, for example, found across the NW-SE striking fault EFG-16 and it is therefore assumed that this fault was active during the Badenian (and possibly already Karpatian) and represents a long-live structure that influenced the tectono-stratigraphic evolution of the studied southern Vienna Basin. Small onlaps of seismic reflectors that are interpreted in the Badenian package reflect pronounced existing palaeotopography prior to its deposition, possibly resulting from Karpatian faulting or older tectonic events.

Additionally, faults that belong to LFS group also record thickness changes of the Badenian and Sarmatian packages, and to lesser extent also the Pannonian package. The faults (e.g., LFS-3) are interpreted as one of the most important large-scale faults that controlled the deposition during Miocene times. Thickness changes in Badenian and Sarmatian packages related to the syn-sedimentary fault activity are also identified on the 2D lines and best visible on E-W and SW-NE trending lines (e.g., Figure 32).

Faults, which were assigned to the Graben system fault zone (GS) also record changes in thickness. Similarly, to the previously mentioned faults, the Badenian and Sarmatian packages reflect stratal wedging towards a number of faults from the group GS. The growth strata are best imaged outside the central graben, i.e., along eastern flanks of the graben (Figure 30).

5.2 Evolution of the depocenters

Constructed time-thickness maps in Figures 14-16 illustrate locations of existing depocenters during individual Miocene intervals and their shift through time. During Badenian times, the depocenters are interpreted to be isolated, possibly with reduced inter-connections and maximum thickness over 800 ms (TWT). Four extensive, probably isolated Badenian depocenters were located in the N and NE. This corresponds to the interpretation that the GS faults that controlled the northern segment of the central graben, EFG faults in that NE region, and also the N-S trending faults belonging to the LFS group record significant syn-sedimentary activity. Interestingly, the Mannersdorf Horst seems to separate the two most easterly located depocenters (Figure 14).

In the Sarmatian, the shift of depocenter to the NW and formation of one extensive depocenter that is controlled by the LFS faults is apparent (Figure 15). It is noted that the Mannersdorf Horst was buried by that time and did not form a positive feature which would act as a barrier. Further, the northern segment indicates reduced fault activity when compared to the Badenian interval.

In Pannonian times, the extensive depocenter shifted westwards, probably being continuously controlled by the long-term active Leopoldsdorf Fault system. Another, much smaller depocenter developed in the south, roughly in the northern part of the Mitterndorf Basin (Figure 16). This implies syn-sedimentary activity of the faults that controlled the southern segment of the central graben (GS).

5.3 Structural setting of the area

The regional extent of the data used in this study allowed for the identification of four main fault groups. Undoubtedly, and in full agreement with previously published studies, the Leopoldsdorf Fault system (LFS) played an important role in structuring of the southern Vienna Basin during Miocene. The integration of 2D and 3D data enabled detailed mapping of LFS geometry including the linkage of this group to the faults of the GS within the 3D data set (Figure 17). The data shows that the LFS branches off at a nearly 90° angle from the GS and further north it migrates westwards and northwards. The LF is characterized by its steep, deep reaching normal faults that show general N-S strike.

The Eastern Fault Group (EFG), although much smaller in size, and the Leopoldsdorf Fault System (LFS) show a very similar strike direction (Figure 17). It is proposed here that N-S trending faults from both groups are offset by the NE-SW trending faults of the Graben System (GS) leading to the conclusion that GS could be a younger fault system than the LFS and EFG. It is plausible to assume that EFG faults might be older or of similar age as the LFS fault group.

The Western Fault Group (WFG) (Figure 17) represents a small, locally constricted and significant fault zone that could be an antithetic fault zone adjusting to the LFS indicated by the main strike directions of its faults.

The steeply dipping faults that represent the basin-bounding faults of the central graben with its two main segments (GS) record syn-sedimentary Miocene activity with possibly switching activity among the basin-bounding faults throughout the Miocene intervals. A negative flower structure (shown e.g., in Figures 23 and 26), and also described by Hinsch et al. (2005a,b,c), is the major structural element that is characteristic for the central graben (GS) and documents oblique-slip motion along the VBTF in the southern Vienna Basin.

It is believed that the interpretation of regional seismic horizons, the construction of time-thickness maps as well as detailed fault interpretation have resulted in a better understanding of the processes, which controlled the tectono-stratigraphic evolution of the southern Vienna Basin during Miocene times.

Chapter 6: Conclusions

1) The combination of 2D and 3D seismic data allowed a more detailed regional mapping of faults and stratigraphic elements in the southern Vienna Basin. It resulted in the identification of four major fault groups with contrasting locations, strikes and sizes. Three of these groups, namely LFS, GS and EFG, span throughout the 2D lines and the 3D cube, while the fourth, WFG group, is only interpreted on 2D Lines.

2) The time-thickness maps constructed for the Badenian, Sarmatian and Pannonian packages clearly demonstrate a lateral shift in depocenters throughout corresponding time intervals. The deposition of sediments was focused in the N and NE during the Badenian in four individual depocenters, while it shifted north-westwards during the Sarmatian forming one single depocenter. The Panonnian time-thickness map exhibits a westward shift of the depocenter and the development of a smaller depocenter in the south, in the northernmost part of the Mitterndorf Basin.

3) Stratal thickness changes are interpreted to occur within the Badenian, Sarmatian and Pannonian packages. These changes most probably indicate syn-sedimentary fault activity. The Karpatian package, which can only be clearly defined in the E and NE, exhibits more subtle thickness changes pointing to the conclusion that syn-sedimentary faulting also controlled the deposition during this period.

4) The Leopoldsdorf Fault system (LFS) branches off the Vienna Basin Transfer Fault, also known as VBTF. The Leopoldsdorf Fault is linked to the major NE-SW trending faults of the Graben System (GS) in the south of the studied area (3D data), but swings westwards and changes its strike to the N-S further north (2D and 3D data). In general, the majority of the interpreted faults have steep dips and record long-term and short-term syn-sedimentary activity during individual Miocene intervals.

5) The two major segments of the central graben (GS) exhibit opposite polarity. The southern segment is characterised by strata dipping to the SE, while the Miocene strata in the northern segment dip to the NW.

Acknowledgments

First of all, I want to thank my supervisors Dr. Kateřina Schöpfer and Dr. Kurt Decker for their patient and intensive support and help throughout the process of writing this thesis. They allowed me to work independently and take my time during these tumultuous times but were always ready to help and support me.

Secondly, I would like to thank my parents, for without them it would not have been possible to finish my studies in a carefree and lighthearted way to enjoy the experiences of university.

Finally, I would like to thank Philipp Strauss and OMV Vienna for providing the data and making this thesis possible.

References

Beidinger, A., & Decker, K. (2011). 3D geometry and kinematics of the Lassee flower structure: Implications for segmentation and seismotectonics of the Vienna Basin strike–slip fault, Austria. Tectonophysics, 499(1-4), 22-40.

Decker, K. (1996). Miocene tectonics at the Alpine-Carpathian junction and the evolution of the Vienna Basin. Mitt. Ges. Geol. Bergbaustud. Österr, 41, 33-44.

Decker, K., Peresson, H., & Hinsch, R. (2005). Active tectonics and Quaternary basin formation along the Vienna Basin Transform fault. Quaternary Science Reviews, 24(3-4), 305-320.

Fodor, L. (1995). From transpression to transtension: Oligocene-Miocene structural evolution of the Vienna basin and the East Alpine-Western Carpathian junction. Tectonophysics, 242(1-2), 151-182.

Gutdeutsch, R., & Aric, K. (1988). Seismicity and Neotectonics of the East Alpine-Carpathian and Pannonian Area: Chapter 15

Hinsch, R., Decker, K., & Peresson, H. (2005). 3-D seismic interpretation and structural modeling in the Vienna Basin: implications for Miocene to recent kinematics. Austrian Journal of Earth Sciences, 97, 38-50.

Hinsch, R., Decker, K., & Wagreich, M. (2005a). 3-D mapping of segmented active faults in the southern Vienna Basin. Quaternary Science Reviews, 24(3-4), 321-336.

Hinsch, R., Decker, K., & Wagreich, M. (2005b). A short review of Environmental Tectonics of the Vienna Basin and the Rhine Graben area. Austrian Journal of Earth Sciences, 97(2004).

Hintersberger, E., Decker, K., Lomax, J., & Lüthgens, C. (2018). Implications from palaeoseismological investigations at the Markgrafneusiedl Fault (Vienna Basin, Austria) for seismic hazard assessment. Natural Hazards and Earth System Sciences, 18(2), 531-553.

Hölzel, M., Decker, K., Zámolyi, A., Strauss, P., & Wagreich, M. (2010). Lower Miocene structural evolution of the central Vienna Basin (Austria). Marine and Petroleum Geology, 27(3), 666-681.

Hölzel, M., Wagreich, M., Faber, R., & Strauss, P. (2008). Regional subsidence analysis in the Vienna basin (Austria). Austrian Journal of Earth Sciences, 101.

Kováč, M., Baráth, I., Harzhauser, M., Hlavatý, I., & Hudáčková, N. (2004). Miocene depositional systems and sequence stratigraphy of the Vienna Basin. Courier Forschungsinstitut Senckenberg, 246, 187-212.

Kreutzer N. (1992). Matzen field – Austria, Vienna Basin. Amer. Assoc. Petrol. Geol. Treatise-Atlas. Structural Traps 7, 57-93.

Lee, E. Y., & Wagreich, M. (2016). 3D visualization of the sedimentary fill and subsidence evolution in the northern and central Vienna Basin (Miocene). Austrian Journal of Earth Sciences, 109(2), 241-251.

Lee, E. Y., & Wagreich, M. (2017). Polyphase tectonic subsidence evolution of the Vienna Basin inferred from quantitative subsidence analysis of the northern and central parts. International Journal of Earth Sciences, 106(2), 687-705.

Peresson, H., & Decker, K. (1996). From extension to compression: Late Miocene stress inversion in the Alpine-Carpathian-Pannonian transition area. Mitt Ges Geol Bergbaustud Österr, 41, 75-86

Piller W.E. 1999. The Neogene of the Vienna Basin. Berichte der Geologischen Bundesanstalt, v. 49, p. 11-19.

Salcher, B. C. (2008). Sedimentology and modelling of the Mitterndorf Basin (Doctoral dissertation, uniwien).

Salcher, B. C., Meurers, B., Smit, J., Decker, K., Hölzel, M., & Wagreich, M. (2012). Strike-slip tectonics and Quaternary basin formation along the Vienna Basin fault system inferred from Bouguer gravity derivatives. Tectonics, 31(3).

Sauer, R., Seifert, P. and Wessely, G., (1992). Part I: Outline of Sedimentation, Tectonic Framework and Hydrocarbon Occurrence in Eastern Lower Austria. Mitteilungen der Österreichischen Geologischen Gesellschaft, 85, 5–96.

Seifert, P. (1996). Sedimentary-tectonic development and Austrian hydrocarbon potential of the ViennaBasin. In: Wessely G- & Liebl W. (Eds.): Oil and gas in Alpidic thrustbelts and basins of central and eastern Europe. EAGE Spec. Publ. 5, 331-341.

Strauss, P., Harzhauser, M., Hinsch, R., & Wagreich, M. (2006). Sequence stratigraphy in a classic pull-apart basin (Neogene, Vienna Basin). A 3D seismic based integrated approach. GEOLOGICA CARPATHICA-BRATISLAVA-, 57(3), 185.

Vail, P.R., Mitchum, R.M. and Thompson, S., 1977. Seismic stratigraphy and global changes of sea level, Part 4: Global Cycles of relative changes of sea level. Am.Assoc.Petrol.Geol., Mem., 26: 83-97.

Wagreich, M., & Schmid, H. P. (2002). Backstripping dip-slip fault histories: apparent slip rates for the Miocene of the Vienna Basin. Terra Nova, 14(3), 163-168.

Wessely, G., Kröll, A., Jiříček, R. and Nemec, F., (1993). Wiener Becken und angrenzende Gebiete-Geologische Einheiten des präneogenen Beckenuntergrundes. Geologische Themenkarte der Republik Österreich 1:200.000, Geologische Bundesanstalt, Vienna.

Wessely, G. (2006). Geologie der Österreichischen Bundesländer Niederösterreich. Geologische Bundesanstalt, Vienna.